AD-A084 653 BERKELEY RESEARCH ASSOCIATES INC CA F/G 20/9
A POWER MODEL FOR PLASMA CONVECTION.(U)
APR 79 J B WORKMAN, S Y CHU, J R FERRANTE DNA001-78-C-0092
UNCLASSIFIED PD-BRA-79-201 DNA-4927F NL

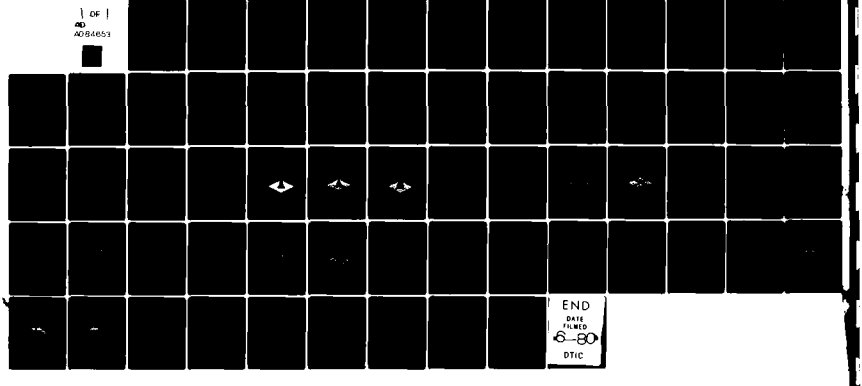

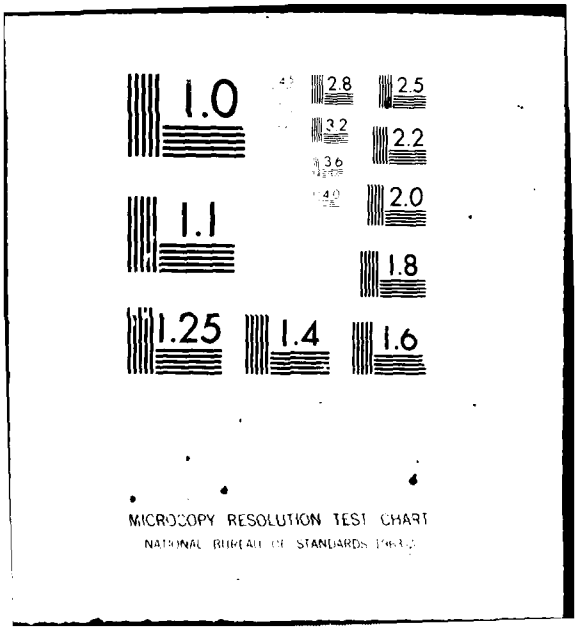
1.0
2.8
2.5
3.2
2.2
3.6
4.0
2.0
1.1
1.8
1.25
1.4
1.6
MICROCOPY RESOLUTION TEST CHART
NATIONAL BUREAU OF STANDARDS

DNA 4927F

A POWER MODEL FOR PLASMA CONVECTION

Berkeley Research Associates, Inc.
P.O. Box 983
Berkeley, California 94701

1 April 1979

Final Report for Period 1 January 1978—31 March 1979

CONTRACT No. DNA 001-78-C-0092

APPROVED FOR PUBLIC RELEASE;
DISTRIBUTION UNLIMITED.

THIS WORK SPONSORED BY THE DEFENSE NUCLEAR AGENCY
UNDER RDT&E RMSS CODE B322078464 S99QAXHC04116 H2590D.

Prepared for
Director
DEFENSE NUCLEAR AGENCY
Washington, D. C. 20305

Destroy this report when it is no longer needed. Do not return to sender.

PLEASE NOTIFY THE DEFENSE NUCLEAR AGENCY, ATTN: STTI, WASHINGTON, D.C. 20305, IF YOUR ADDRESS IS INCORRECT, IF YOU WISH TO BE DELETED FROM THE DISTRIBUTION LIST, OR IF THE ADDRESSEE IS NO LONGER EMPLOYED BY YOUR ORGANIZATION.

UNCLASSIFIED

SECURITY CLASSIFICATION OF THIS PAGE *(When Data Entered)*

REPORT DOCUMENTATION PAGE		READ INSTRUCTIONS BEFORE COMPLETING FORM
1. REPORT NUMBER DNA 4927F	2. GOVT ACCESSION NO. AD-A084653	3. RECIPIENT'S CATALOG NUMBER
4. TITLE *(and Subtitle)* A POWER MODEL FOR PLASMA CONVECTION		5. TYPE OF REPORT & PERIOD COVERED Final Report for Period 1 Jan 78—31 Mar 79
		6. PERFORMING ORG. REPORT NUMBER PD-BRA-79-201
7. AUTHOR(s) Joseph B. Workman S. Y. Frank Chu John R. Ferrante		8. CONTRACT OR GRANT NUMBER(s) DNA 001-78-C-0092
9. PERFORMING ORGANIZATION NAME AND ADDRESS Berkeley Research Associates, Inc. P.O. Box 983 Berkeley, California 94701		10. PROGRAM ELEMENT, PROJECT, TASK AREA & WORK UNIT NUMBERS Subtask S99QAXHC041-16
11. CONTROLLING OFFICE NAME AND ADDRESS Director Defense Nuclear Agency Washington, D.C. 20305		12. REPORT DATE 1 April 1979 13. NUMBER OF PAGES 62
14. MONITORING AGENCY NAME & ADDRESS*(if different from Controlling Office)*		15. SECURITY CLASS *(of this report)* UNCLASSIFIED 15a. DECLASSIFICATION/DOWNGRADING SCHEDULE

16. DISTRIBUTION STATEMENT *(of this Report)*

Approved for public release; distribution unlimited.

17. DISTRIBUTION STATEMENT *(of the abstract entered in Block 20, if different from Report)*

18. SUPPLEMENTARY NOTES

This work sponsored by the Defense Nuclear Agency under RDT&E RMSS Code B322078464 S99QAXHC04116 H2590D.

19. KEY WORDS *(Continue on reverse side if necessary and identify by block number)*

Nuclear Effects
Striations
Plasma Microstructure
Gradient Drift
Plasma Convection

20. ABSTRACT *(Continue on reverse side if necessary and identify by block number)*

A model for simulating the convection of plasma microstructure has been constructed. Labeled 'striation convection,' the procedure is based on the conservation of the square of plasma density or 'plasma power'. The model is driven by a previously developed gradient drift microstructure model. Integrated with other plasma numerical routines, simulation results for several two-dimensional F-layer scenarios are presented.

DD FORM 1 JAN 73 1473 EDITION OF 1 NOV 65 IS OBSOLETE

UNCLASSIFIED

SECURITY CLASSIFICATION OF THIS PAGE *(When Data Entered)*

94

TABLE OF CONTENTS

LIST OF ILLUSTRATIONS

SECTION I
INTRODUCTION

The understanding and modelling of plasma convection in the high altitude environment is a central issue in the proper simulation of a realistic nuclear scenario. This paper is principally concerned with the study of a key aspect of the problem which we have chosen to label "striation convection". One distinguishes between usual or macroscopic plasma convection and striation convection because of present day limitations in computational techniques and resources. In principle, there is only a single physics of plasma motion governed by the same hydrodynamics, whether the scale is 1000 km or 1000 cm. In practice, however, we are forced to arbitrarily divide the phenomena into manageable scale size regimes. We treat the large dimensions (limited by the computational grid) directly with a suitable plasma fluid code. For late-time studies, an electrostatic routine is the usual choice. Shorter scales are defined as "striations" and are modelled in various types of auxiliary routines. In previous research and systems analysis, there has been no provision for an independent motion or convection of this small scale plasma. While some previous work has ignored the motion of this plasma altogether, even the most advanced computations have only considered that it will move in an identical manner to the smallest scale plasma that the grid does, in fact, compute. That is, it is assumed that the striations are "imbedded" in the local gross scale plasma and will be carried along by that plasma in a Lagrangian manner.

Even if one were unaware of the detailed physics of the gradient drift mechanism, the present computations would appear to contain an inconsistency. We would observe from the numerical data that plasma features of different densities

would be convecting at different rates. It would thus seem intuitively incorrect that all features below the grid dimension should be treated as a common Lagrangian mass with uniform motion.

If we turn to a direct consideration of the gradient drift physics, it is immediately apparent that to neglect the relative convection of small scale plasma is to actually neglect the gradient drift mechanism itself. It is, after all, the relative slip of different features that produces structure on the fine scale in the first place.

At late times, the process of striation convection has profound effects upon the overall plasma evolution. Both the breakup of large initial features and the dispersal of material to remote locations is governed by the mechanism. It could easily be argued that the process is central to all late-time modelling of plasma evolution. Clearly, without a proper consideration of this convection, all conventional computations of high-altitude plasma motion lead to unphysical results at relatively early times.

In lieu of the ability to carry out "exact" plasma simulations over the vast range of scale sizes actually encompassed in a nuclear scenario, our proposal is to model the plasma in an integral manner by conserving certain key extensive properties. In particular, the modelling will rely on conservation of plasma density and plasma "power". Power is defined as a function of the square of the density, either absolute or as a variance about a local mean. The next section of the paper will explicitly review the construction of the class of power functions to be employed. The use of plasma power to model convection is closely tied to previous work on power modelling of in-situ microstructure. We will reference[1] and make use of previous results in constructing the present model.

Fundamentally, the physics of striation convection produces a differential slip of high and low density plasma within a macroscopic cell. The result is a convective interleaving of high and low density which appears as "mixing" on the grand scale. Mixing is, of course, a diffusive process and, thus, the apparent end result is displayed as plasma diffusion among neighboring macroscopic cells. The process is not to be confused with true crossfield diffusion, but rather is the integrated result of plasma striation interleaving.

The next section of the paper will develop the concept of plasma power and lay the groundwork for the detailed convection model. A subsequent section will outline the actual mixing model and indicate the connection to previously developed microstructure modelling. An appendix will display a simple microstructure model which incorporates recent philosophical changes in the older model and provides a convenient vehicle for testing the mixing concept. The final sections give example computations and conclusions.

SECTION II
PLASMA POWER FORMULATION

It is well known that field line integrated plasma density in the F-layer of the ionosphere is governed by incompressible fluid dynamics for crossfield convection.[2] The relative uniformity of plasma parallel to the field allows a reasonable two-dimensional approximation for modelling transverse microstructure phenomenology. Thence, with the exception of diffusion on the very smallest scale size, the plasma density itself can be modelled as incompressible flow. It follows that, in addition to the density, any function of density becomes a preserved Lagrangian quantity. Of particular interest is the square of plasma density which is equivalent to "plasma power". Previous research[1] has laid the groundwork for the construction of the conservation concepts to be employed here.

For convenience, let us consider a two-dimensional Cartesian space containing a plasma density distribution. The space is sufficiently large that the plasma density is uniform at the boundary for all time periods of interest. The schematic in Figure 1 displays an actual continuous density, $n(x,y)$, by the dashed line and a finite cell representation, $n_o(x,y)$. Denoting the cell dimension as 2L and the total spatial extent as ML, we can construct a variety of conservation relations. For the density itself, we can express the continuous function as

$$\frac{\partial}{\partial t}\left[\iint^{ML} n\, dx\, dy\right] = 0 \qquad (1)$$

$$\frac{D}{Dt}\left[\iint^{2L} n\, dx\, dy\right] = \text{diffusion } (\pm) \qquad (2)$$

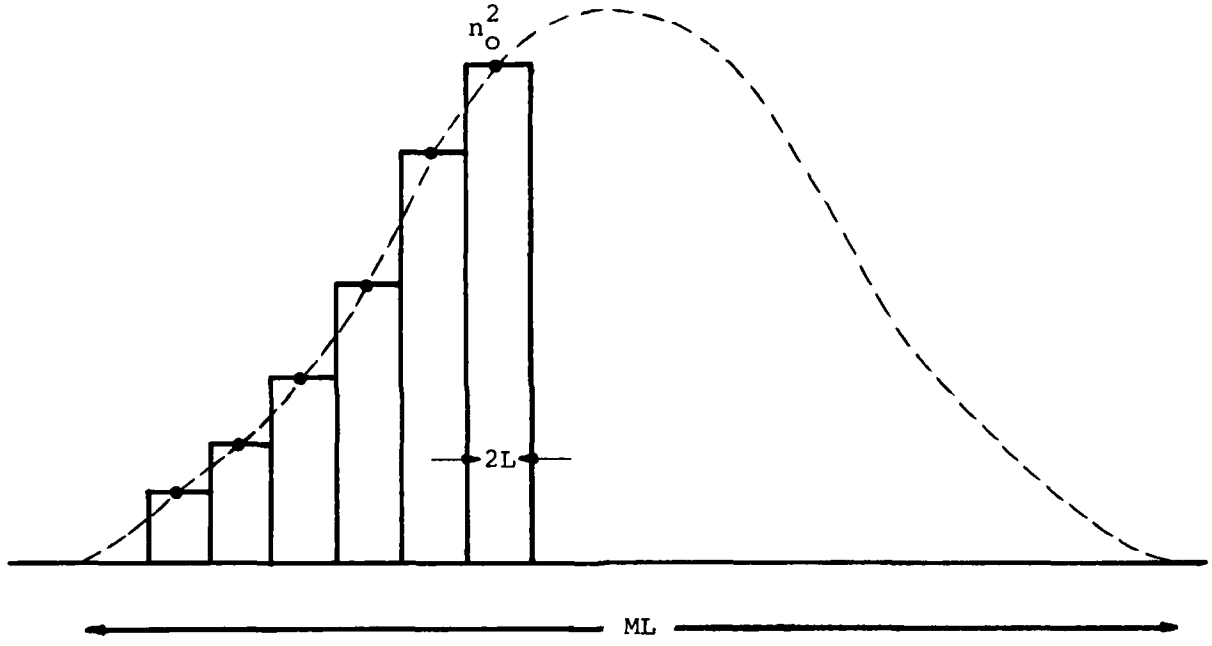

Figure 1. Background power.

In thermodynamic terminology, we shall find that density conservation in gradient drift modelling is analogous to "energy" in conventional fluid turbulence modelling.

For the density square relations, we can write

$$\frac{\partial}{\partial t}\left[\iint^{ML} n^2 \, dx \, dy\right] = -\text{total diffusion} \leq 0 \qquad (3)$$

$$\frac{D}{Dt}\left[\iint^{2L} n^2 \, dx \, dy\right] = \text{local diffusion } (\pm) \qquad (4)$$

To continue the thermodynamic analogy, we will find that density square conservation resembles "inverse entropy".

To introduce the concept of plasma power, let us represent the density as a finite Fourier series

$$n(x,y) = \sum_{k_x,k_y} a(k_x,k_y)\, e^{i\theta(k_x,k_y)}\, e^{ik_x x}\, e^{ik_y y} \qquad (5)$$

where a is the real polar modulus and θ is the plasma phase. The density square representation becomes

$$\frac{1}{M^2L^2}\iint n^2 dx\, dy = \sum_{k_x,k_y} a^2(k_x,k_y) \equiv \Sigma PSD \qquad (6)$$

Thence, the conservation relation which governs all microstructure evolution becomes

$$\frac{D}{Dt}\,[\Sigma PSD]_{2L} = -\left[\begin{matrix}\text{local}\\ \text{diffusion}\end{matrix}\right]_{2L} \qquad (7)$$

where ΣPSD is, of course, the power spectral summation. When referenced to a local mean or detrending curve, it is commonly called the density variance.

An exact, continuous treatment of the evolution of plasma power would provide no simplification over an exact density solution for convection. It is the ability to divide and approximately model various components of the power which makes the general concept useful.[1]

The basic component of power is provided by the macroscopic background. Again, with reference to Figure 1, we can define both a local background power, P_ℓ, and a total background power, P_T

$$P_\ell \equiv n_o^2(x,y)\ 4L^2 \tag{8}$$

$$P_T \equiv \sum^{M^2} P_\ell \tag{9}$$

Note that, in the limit of infinitely small cell size, $2L$, the absolute value of P_ℓ goes to zero. However, M^2 becomes proportionately infinitely large and P_T would give the true total power in the overall space. For finite L, the expression P_T gives only the "background power" with several components remaining to give the true total.

In Figure 2, we focus on an individual cell in order to define components of the "local power". On the left, we describe the "local macro power", P_M, using a linear detrending line of slope, d. Note that the line is drawn to provide no net integrated density. This construction is important to avoid cross terms in defining the power and ease in later adding components of power together.

$$P_M = n_o^2\ 4L^2 \left[1 + \frac{1}{3}\frac{L^2}{d^2}\right] \tag{10}$$

or

$$P_M = P_\ell(1 + F_o) \tag{10a}$$

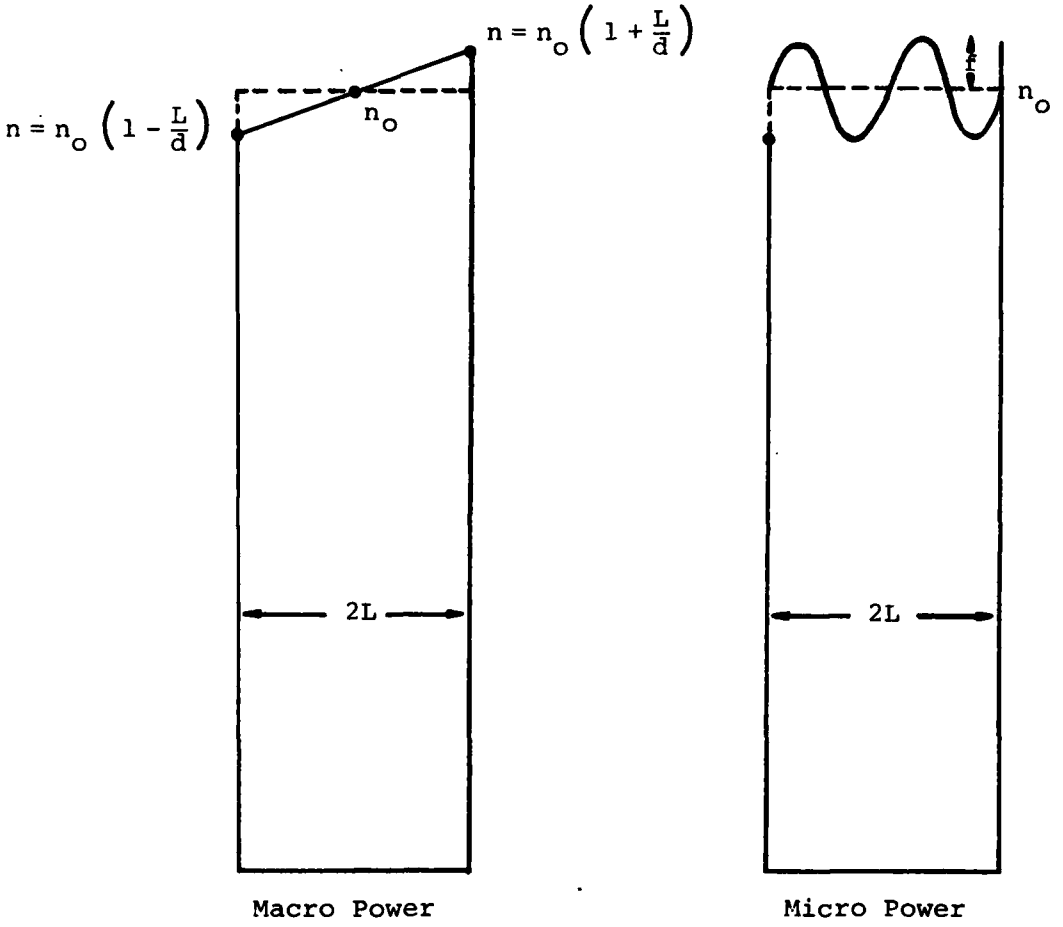

Figure 2. Local power components.

where F_o is the local slope power defined as

$$F_o = \frac{1}{3}\frac{L^2}{d^2} \tag{11}$$

Aside from its role in detrending, the quantity F_o is important because we identify it as the local driver of plasma microstructure within the cell. To make a connection with previous work,[1] we can rewrite (11) in terms of a grid cell reference wavenumber k_o as

$$\frac{1}{d} = k_o \sqrt{F_o} \tag{12}$$

Note that $k_o\sqrt{F_o}$ is independent of cell size, as one would expect of a true physical quantity. The value of F_o, however, will disappear and play no role in power conservation, if L is made infinitely small. Thus, F_o is a model-dependent artifice which provides one component of the density variance within a grid cell.

For illustration purposes, we have oriented the slope along a particular face of a square cross-section cell. Obviously, in general, a given cell will demand a detrending slope surface at some angle to the natural cross section. In application, the modelling allows an arbitrary orientation of the slope surface. The peculiar intersections between cells are not considered, of course, and provide one of several sources of inconsistency common to finite difference formulations.

On the right-hand side of Figure 2, we focus on the remaining plasma power defined as "local micro power". This quantity is treated as a normalized power spectral summation denoted by F_C.

$$F_C = \sum f^2 \tag{13}$$

The general formulation and spectral characteristic of this quantity have been discussed in previous work.[1] The specific simplifications that will be employed in the present study are shown in the Appendix. The major assumption concerning this component of power is the use of a single one-dimensional spectrum with modulus amplitudes, f , to represent all orientations of the general transform with modulus amplitudes, a .

In summary, we note that the total power in a cell, P_{ℓ_Σ} , is given by

$$P_{\ell_\Sigma} \equiv P_\ell(1 + F_o + F_C) \tag{14}$$

and the total power in the entire space, P_{T_Σ} , is given by

$$P_T \equiv \sum^{M^2} P_{\ell_\Sigma} \tag{15}$$

Again, it is important to remember that the components F_o and F_C arise only because of finite gridding.

In the next section, we will employ this plasma power formulation to construct a microstructure convection model.

SECTION III
THE MIXING MODEL

The gradient drift convection of microscopic features produces an effective interleaving of plasma between neighboring macroscopic cells, as shown in Figure 3. When viewed from the standpoint of macroscopic plasma power, the net effect of the interleaving is to reduce the combined power of the cells. The simple schematic of Figure 4 illustrates the point.

In part A of Figure 4, we display a simple pair of adjacent cells before convection. Each has the same area, A, but different and uniform background densities, n_1 and n_2. In part B, we interchange equal pieces of area A' and corresponding densities, commensurate with imcompressible microscopic interleaving. The proper cell boundary is now structured as shown. Finally, in part C, we redraw the original grid boundary and construct new average or "mixed" densities, n_1' and n_2'.

Prior to interleaving the combined cell power, P_C may be stated as

$$P_C = \left(n_1^2 + n_2^2\right) 4L^2 \tag{16}$$

After interleaving, the power becomes

$$\begin{aligned} P_C' &= \left(n_1'^2 + n_2'^2\right) 4L^2 \\ &= (n_1 - \delta n_1 + \delta n_2)^2 \, 4L^2 \\ &\quad + (n_2 - \delta n_2 + \delta n_1)^2 \, 4L^2 \end{aligned} \tag{17}$$

where $\delta = A'/A$ and $A = 4L^2$.

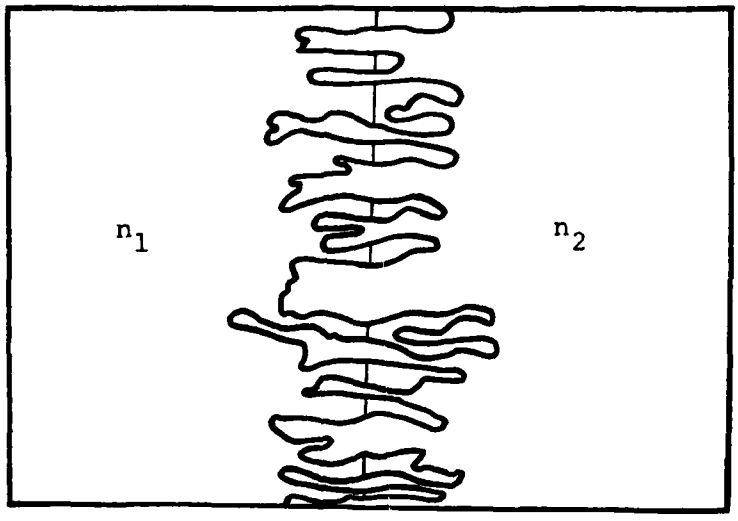

Figure 3. Striation interleaving between macro cells.

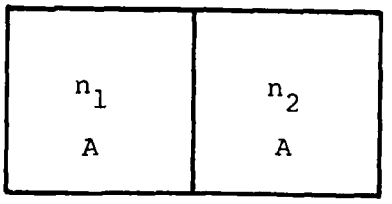

A. Macro grid before interleaving.

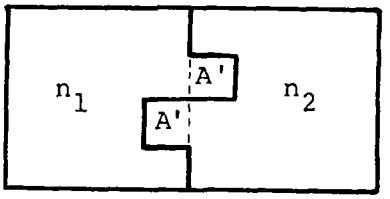

B. Idealized interleaving.

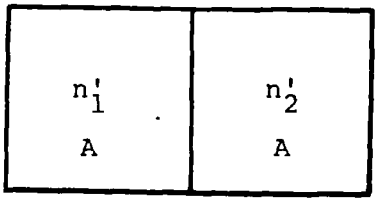

B. Regridded macro cells
with new mixed densities.

Figure 4. Interleaving and regridding.

The change in macroscopic power ΔP_C is then

$$\Delta P_C = P_C' - P_C = -2(\delta-\delta^2)(n_1-n_2)^2\, 4L^2 \qquad (18)$$

We should note that geometry prevents δ from exceeding 1/2 (the maximum power loss in the pair).

Initially, the defined microscopic power, P_M, is zero. After mixing, referenced to the new primed macroscopic cell densities, it would be computed as

$$P_M' = \frac{(n_2-n_1')^2\, A' + (n_1-n_1')^2\, (A-A')}{A}\, 4L^2$$

$$+ \frac{(n_1-n_2')^2\, A' + (n_2-n_2')^2\, (A-A')}{A}\, 4L^2 \qquad (19)$$

Substitution and reordering reduces to

$$P_M' = 2(\delta-\delta^2)(n_1-n_2)^2\, 4L^2 \qquad (20)$$

The change in microscopic power is, thus, identically

$$\Delta P_M = P_M' - P_M = -\Delta P_C \qquad (21)$$

Overall total power has been conserved, but macroscopic power has been lost in the exact amount equal to microscopic power gain. This equality and conservation forms the basis for the mixing model.

We have constructed a simple, but physically reasonable, mixing model by considering the interaction between a cell and its closest four neighbors. The five-point "cross" that results is shown in Figure 5. Eventually, it may be necessary to employ a more elaborate 13-point model to provide better symmetry and properly treat the slope power component. For

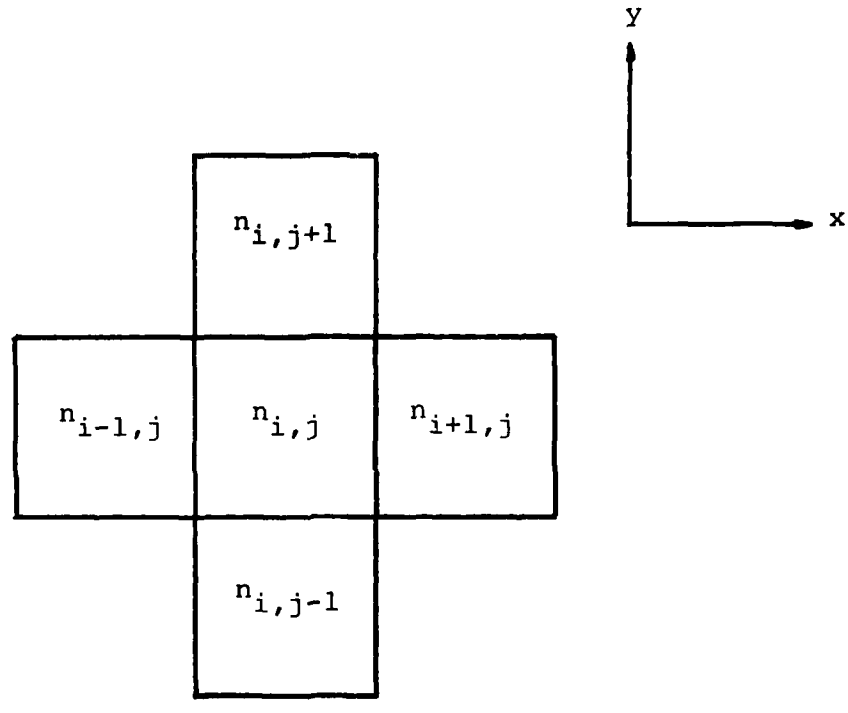

Figure 5. Simple mixing model.

the present, however, we believe that the simple model is adequate to account for the basic physics and explore the resultant phenomenology.

The total background power in the cells of Figure 5 is given by

$$P_C = 4L^2(n_{i,j}^2 + n_{i+1,j}^2 + n_{i-1,j}^2 + n_{i,j+1}^2 + n_{i,j-1}^2) \tag{22}$$

Prior to a mixing step, we can define the density differences between cells as

$$\begin{aligned} \Delta_1 &= (n_{i,j} - n_{i-1,j})_o \\ \Delta_2 &= (n_{i,j} - n_{i+1,j})_o \\ \Delta_3 &= (n_{i,j} - n_{i,j-1})_o \\ \Delta_4 &= (n_{i,j} - n_{i,j+1})_o \end{aligned} \tag{23}$$

After a mixing step, the new cell densities may be expressed as

$$\begin{aligned} n_{i-1,j} &= (n_{i-1,j})_o + T_x\Delta_1 \\ n_{i,j} &= (n_{i,j})_o - T_x(\Delta_1 + \Delta_2) - T_y(\Delta_3 + \Delta_4) \\ n_{i+1,j} &= (n_{i+1,j})_o + T_x\Delta_2 \\ n_{i,j-1} &= (n_{i,j-1})_o + T_y\Delta_3 \\ n_{i,j+1} &= (n_{i,j+1})_o + T_y\Delta_4 \end{aligned} \tag{24}$$

where the transfer fractions, T_x and T_y are analogous to the simple fraction δ in the earlier example. The actual mixing, of course, occurs between cells aligned with the slip

velocity vector between neutral and ion motion. The quantities T_x and T_y are merely components defined for convenience in the specific coordinate system. We can readily define a single scalar mixing parameter, α, by relating the transfer to the slip components.

$$T_x = \left[\frac{(U_x - V_x)^2}{(U_x - V_x)^2 + (U_y - V_y)^2} \right]^{1/2} \alpha = S\alpha$$

$$T_y = \left[\frac{(U_y - V_y)^2}{(U_y - V_y)^2 + (U_y - V_y)^2} \right]^{1/2} \alpha = C\alpha \qquad (25)$$

The U's are the macroscopic plasma velocity as determined by the usual macroscopic potential solver[2] and the V's are the neutral wind velocity.

Substituting (23) and (25) into (24) and thence into (22) gives the new cell power after a mixing step. Subtracting this power from the initial power provides an expression for the macroscopic power loss during a time step.

$$-\Delta P_C = \Big[2S^2\alpha^2(\Delta_1^2 + \Delta_2^2 + \Delta_1\Delta_2) + 2C^2\alpha^2(\Delta_3^2 + \Delta_4^2 + \Delta_3\Delta_4) + 2SC\alpha^2(\Delta_1 + \Delta_2)(\Delta_3 + \Delta_4) - 2S\alpha(\Delta_1^2 + \Delta_2^2) - 2C\alpha(\Delta_3^2 + \Delta_4^2) \Big] 4L^2 \qquad (26)$$

Now, for each time step for each cell, the quantity $-\Delta P_C(x,y)$ is a known distribution from the solution of the microstructure routine.[1] For the example calculations to be presented in the next section, it is easily expressed from the simple model outlined in the Appendix.

$$-\Delta P_C = \Delta P_M = (n^o_{i,j})^2\ 4L^2$$

$$\times \left[2(\Delta U) k_o \sqrt{F_o}\ F_C + 2\beta_1 (\Delta U) k_o F_o \sqrt{F_o} \left(\frac{k_o}{\bar{k}_C} \right) \right] \Delta t \qquad (27)$$

where Δt is the time step.

At each time step, the relation (26) - (27) is solved to obtain $\alpha(x,y)$ and thence transfer functions T_x and T_y constructed. Both the density distribution, n, and the microscopic power distribution, F_C, are thence mixed to complete the operation.

A complete time step for the plasma consists of the following four operations.

1. Potential solution to obtain U_x, U_y
2. Microscopic power computation
3. Mixing of density and microscopic power
4. Macroscopic convection

In the next section, we will display a series of sample computations and discuss the results.

SECTION IV
EXAMPLE CALCULATIONS AND RESULTS

One of the classic problems in numerical simulation of gradient drift phenomenology is the axisymmetric plasma distribution and wind pattern created by a fireball in a vertical magnetic field. In the absence of striation convection, there is no plasma dynamic mechanism for breaking up and dispersing the cloud. The example calculations, to be presented here, will focus on a simple representation of that geometry to display the behavior of the convection model when faced with this classic configuration.

Each of the three examples will begin with an initial Gaussian plasma density distribution of the form

$$n = 4e^{-\left(\frac{\vec{r}-\vec{r}_C}{r_o}\right)^2} + 1 \qquad (28)$$

where the density, n, is obviously normalized to a uniform background and the r's are the various radii. In all cases, the Gaussian radius, r_o, will be 100 units. The unit dimension is arbitrary, but may be thought of as a kilometer for convenience. The center position, $\vec{r}_C$, will be zero for the first and third cases, but offset 100 units in the second case.

The computational grid will be a Cartesian (x,y) space of total extent 1000 units on a side divided 32×32. The grid reference dimension, L, is, thus, 15.6 units. These numbers provide an outer scale reference wavenumber, k_R, of .22 and an inner scale reference wavenumber, k_D, of 220. All problems commence with the microstructure power, F_C, set equal to zero.

The wind pattern is fixed in time and the same for each case.

$$\vec{V} = \frac{\vec{r}}{r_o + r} \tag{29}$$

The wind is, thus, radially symmetric with the zero value at the center and growing to one unit per second at large radii. The macroscopic potential is solved in the Neumann mode which transmits plasma across the boundary in the wind direction.

All time steps are ten seconds, which implies three steps per 2L for expected peak velocities of one unit per second. The time interval appears adequate for the first two cases, but is perhaps a little coarse for the third case (as the results will indicate). The various mesh reductions, necessary for each of the steps corresponding to potential solution, mixing, and convection, utilize alternating sweep techniques. Unphysical, numerical asymmetries can creep into the pattern during a coarse time step in spite of our consistent use of predictor-corrector procedures.

In the first case, the cloud is placed on center with the wind. The initial density contours are as shown in Figure 6A. In all of the 2-D plots, the contour values are shown above the figure and the mesh of letters A to I represent intermediate levels between ascending contours.

In the purely axisymmetric case, there is very little plasma motion until the microstructure has had a chance to build to significant values. The first noticeable effects occur around 600 seconds. Figures 6B and 6C display contours of n and F_C. The toroidal distribution of F_C is the expected pattern, which gives a ring of peak values on the steep outer face of the cloud.

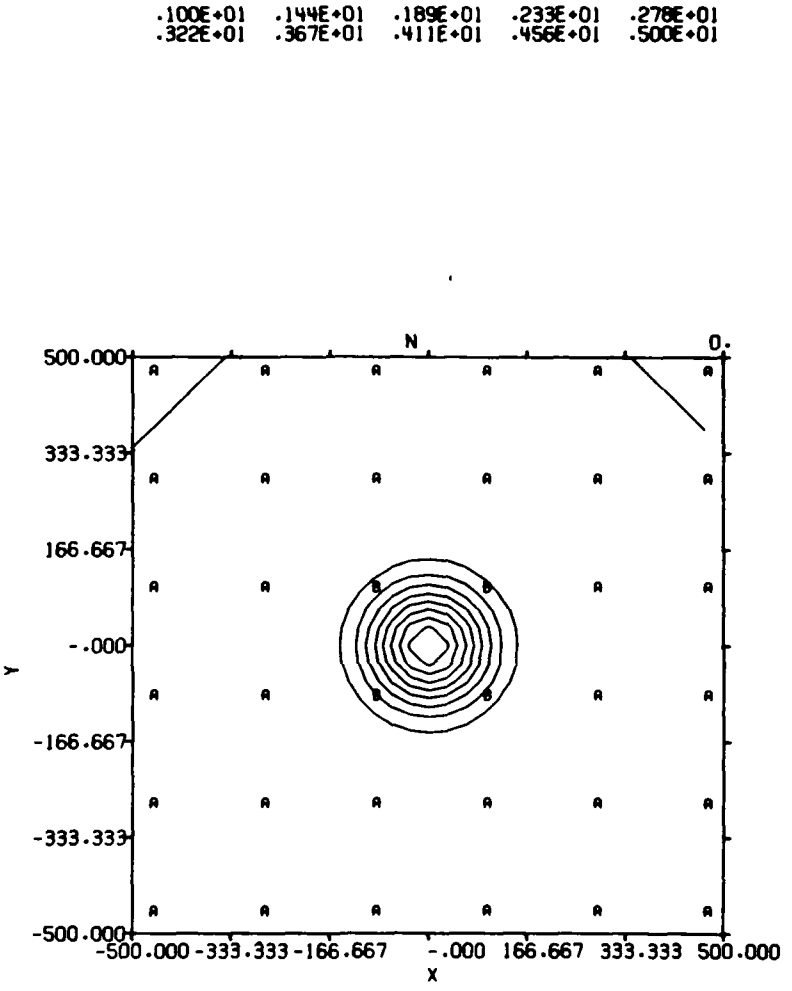

Figure 6A. Case I - plasma density - 0 seconds.

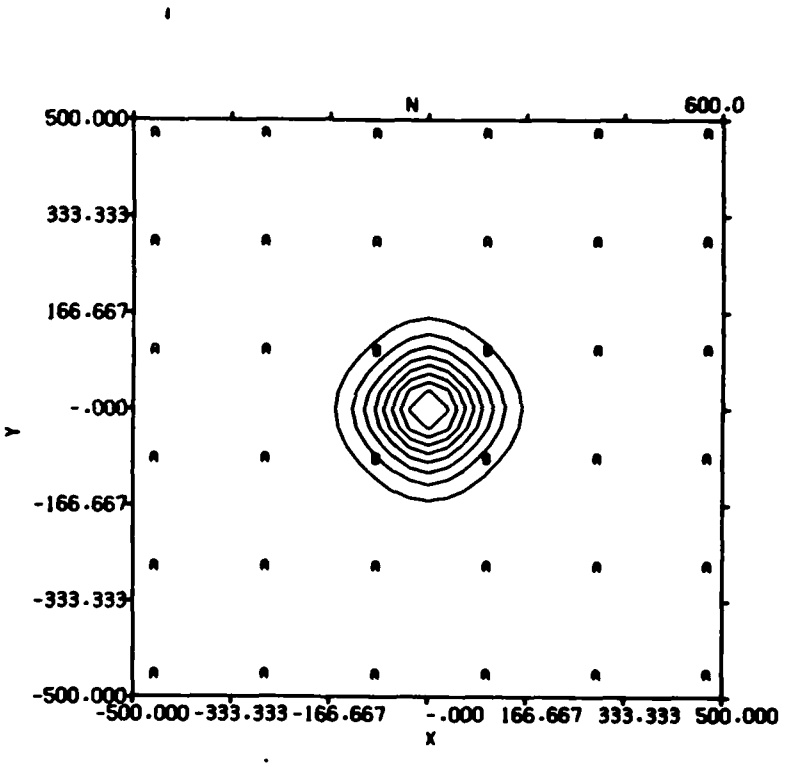

Figure 6B. Case I - plasma density - 600 seconds.

.997E-08 .149E-02 .297E-02 .446E-02 .595E-02
.744E-02 .892E-02 .104E-01 .119E-01 .134E-01

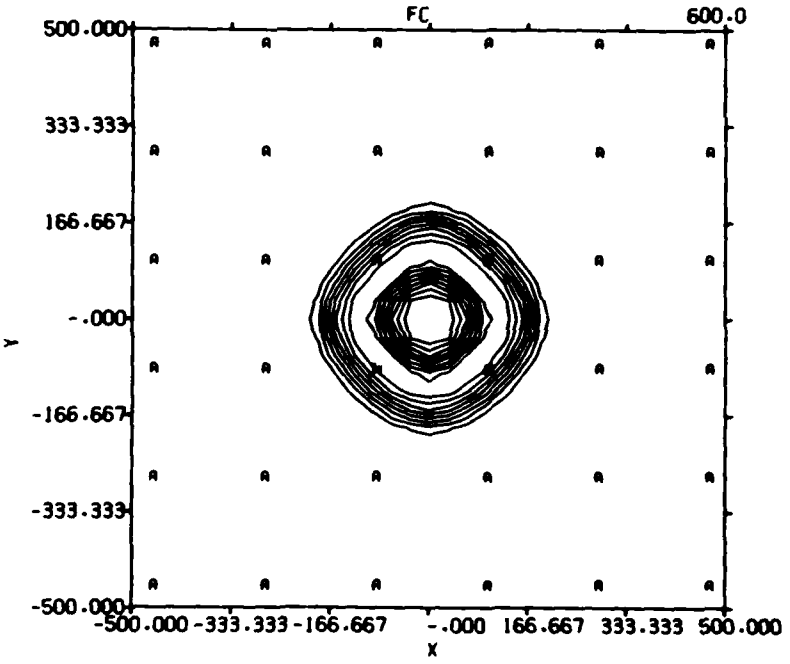

Figure 6C. Case I - microstructure power- 600 seconds
Peak F_C = .0134.

Visualization of the plasma evolution is easiest using 3-D plots and, thus, will be employed for all of the later time development. Figure 6D at 100 seconds shows the density in 3-D prior to any significant motion. Figure 6E at 1000 seconds reflects the initiation of noticeable mixing. The finite cell size and the lack of radial symmetry create the four prongs to the structure. If the gross plasma had possessed any net macroscopic velocity (as in the next case), the prongs would have been washed out. As it is, they emphasize the "cross pattern" of the mixing model. Figures 6F and 6G, at 1300 and 1500 seconds, show the further development of structure. The decline of peak density in the central cloud is evident by this time. By 2000 seconds in Figure 6H, a significant dispersal of plasma has occurred and material is reaching the grid boundary. The remaining plots, Figures 6I, 6J, and 6K, at 2500, 3500, and 6000 seconds, display the final evolution of the plasma. There is complete destruction of the original cloud and dispersal of plasma beyond the grid boundaries.

Fundamentally, the first case demonstrates the overall behavior that one expects from a striation convection model. There are, however, certain obvious deficiencies with respect to the details of the computation. The stationary character of the initial plasma and the lack of complete symmetry in the model combine to produce the cross pattern in the dispersal. Once it is generated, the cross pattern appears to augment itself by serving as a perturbation in the macroscopic potential solver. In a sense, the macroscopic fingers, once produced, may be outrunning the mixing process. The secondary density peaks near the boundary, as in Figures 6H and 6I, would indicate this influence. On the other hand, the mixing does not completely lose its effect, as evidenced by the continuous decline of the peak central density.

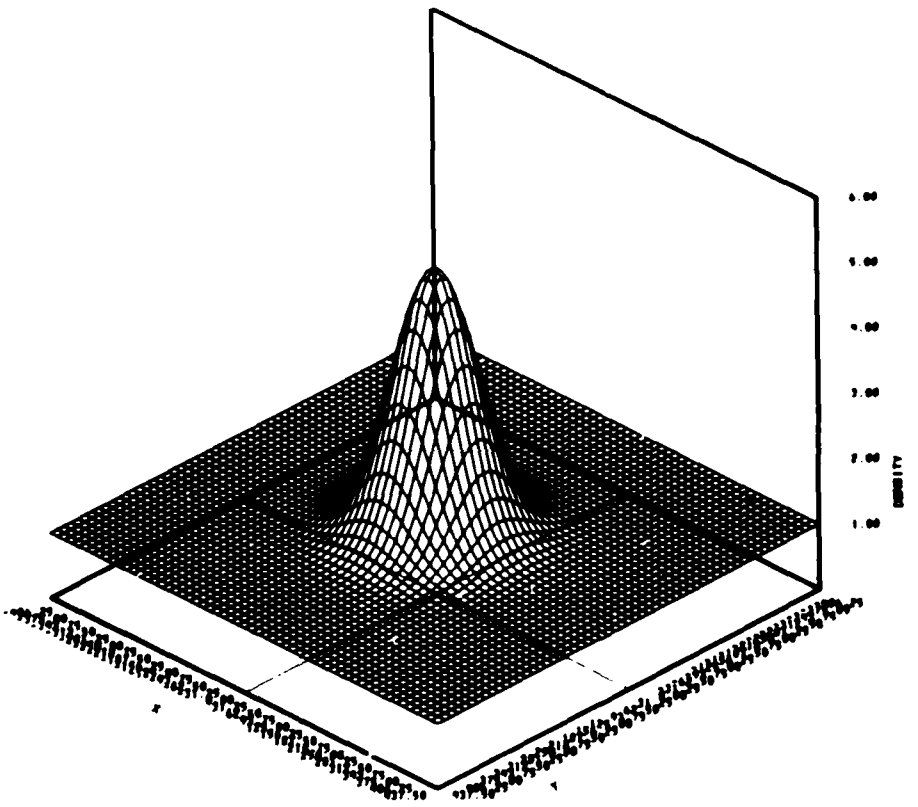

Figure 6D. Case I - plasma density - 100 seconds.

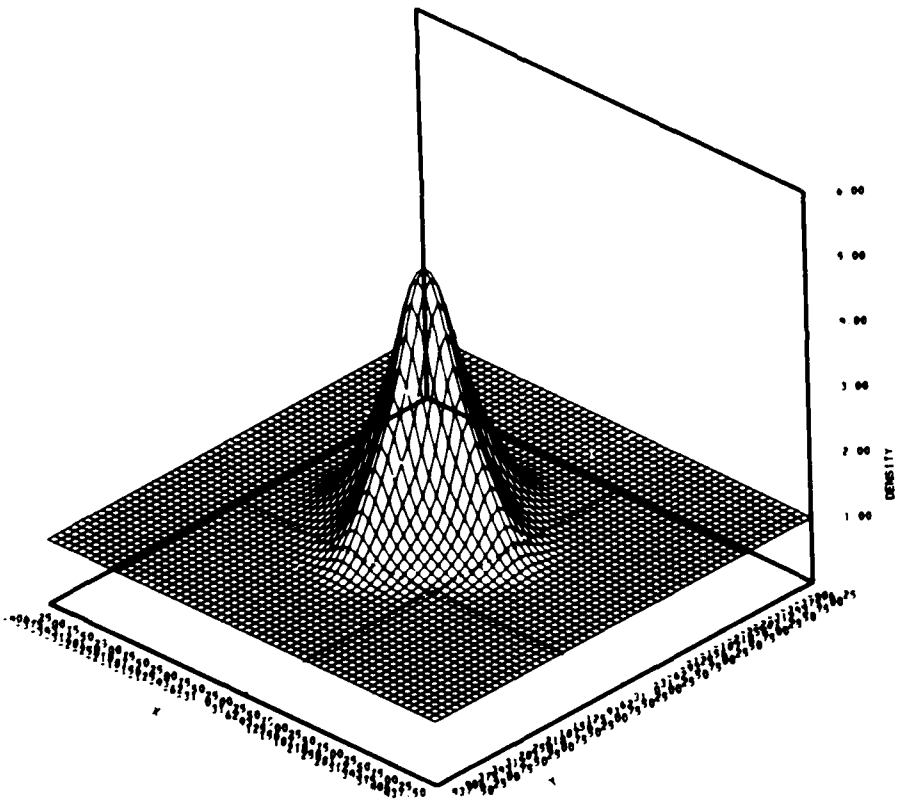

Figure 6E. Case I - plasma density - 1000 seconds.

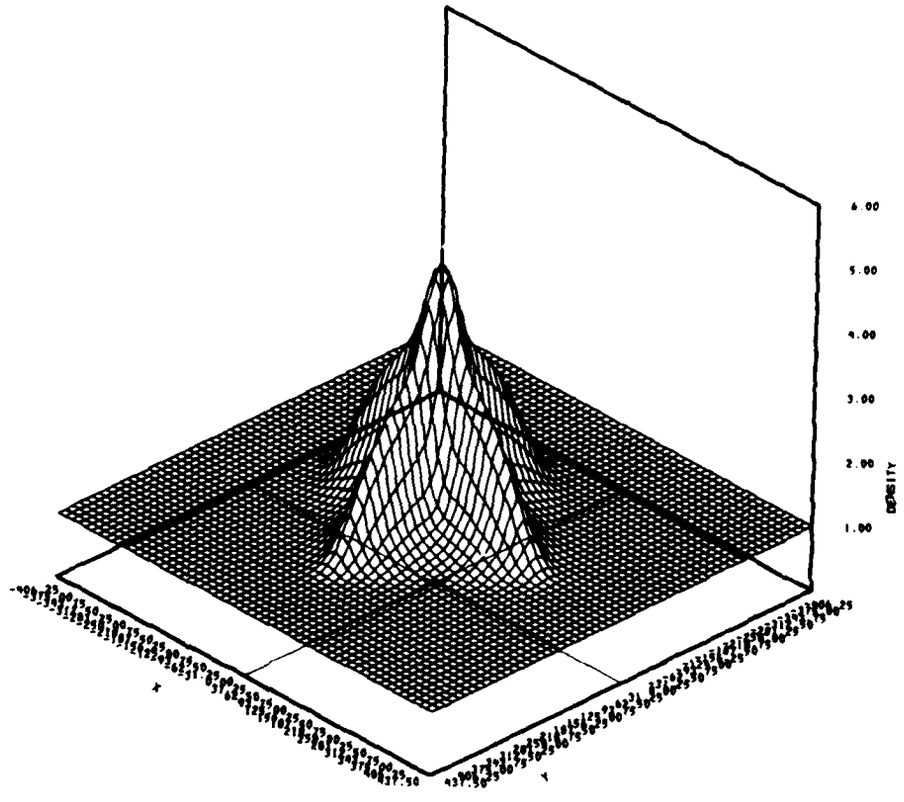

Figure 6F. Case I - plasma density - 1300 seconds.

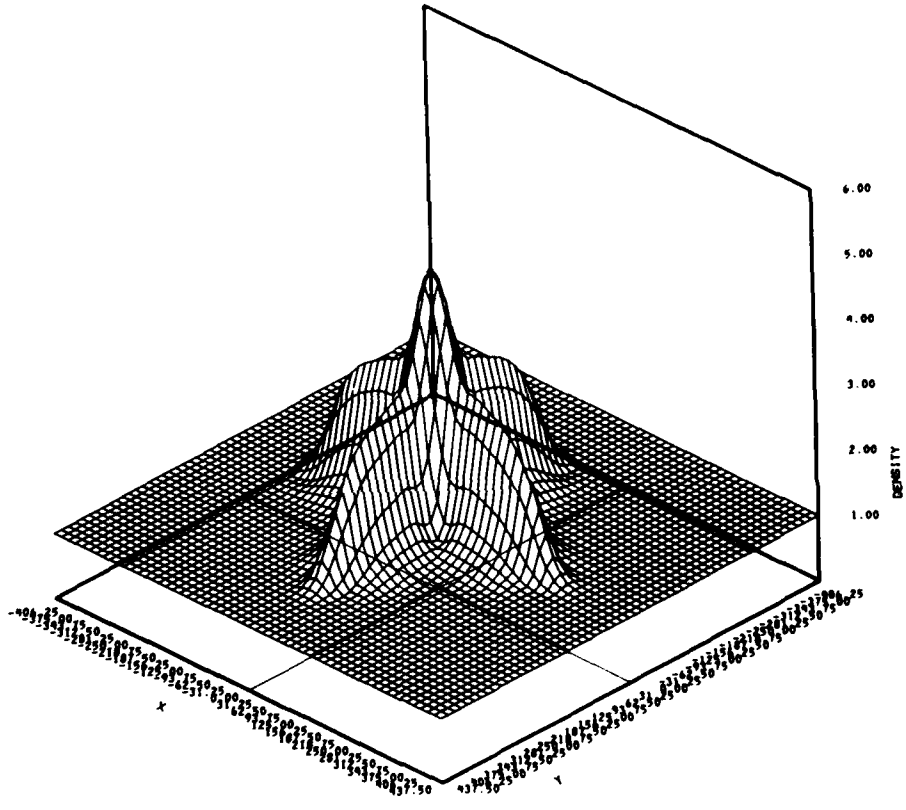

Figure 6G. Case I - plasma density - 1500 seconds.

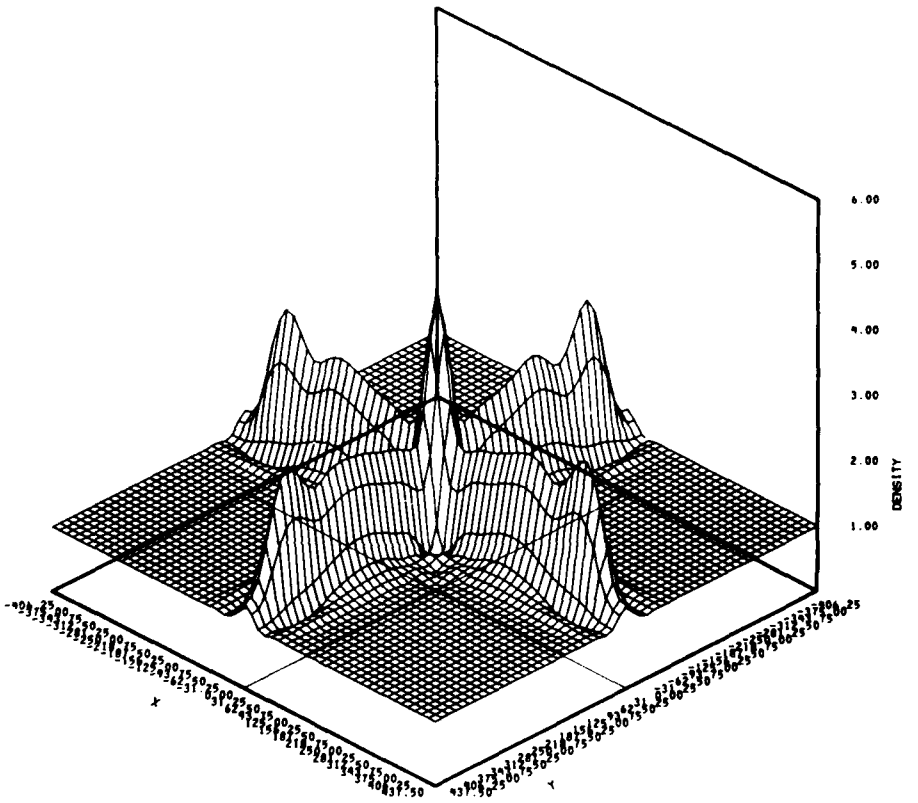

Figure 6H. Case I - plasma density - 2000 seconds.

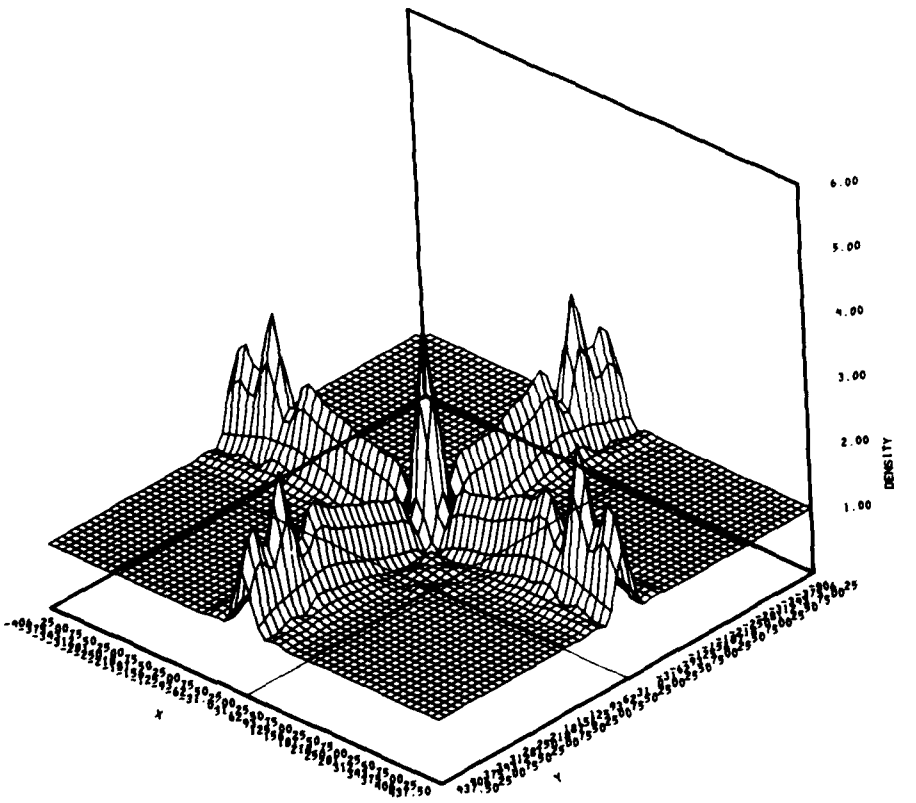

Figure 6I. Case I - plasma density - 2500 seconds.

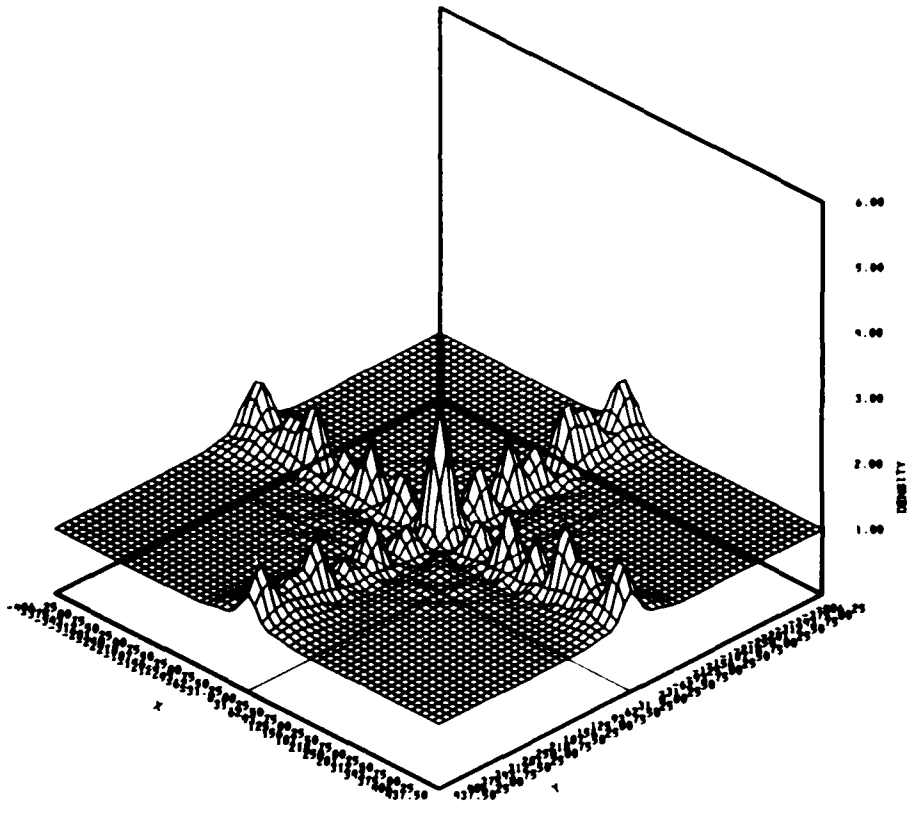

Figure 6J. Case I - plasma density - 3500 seconds.

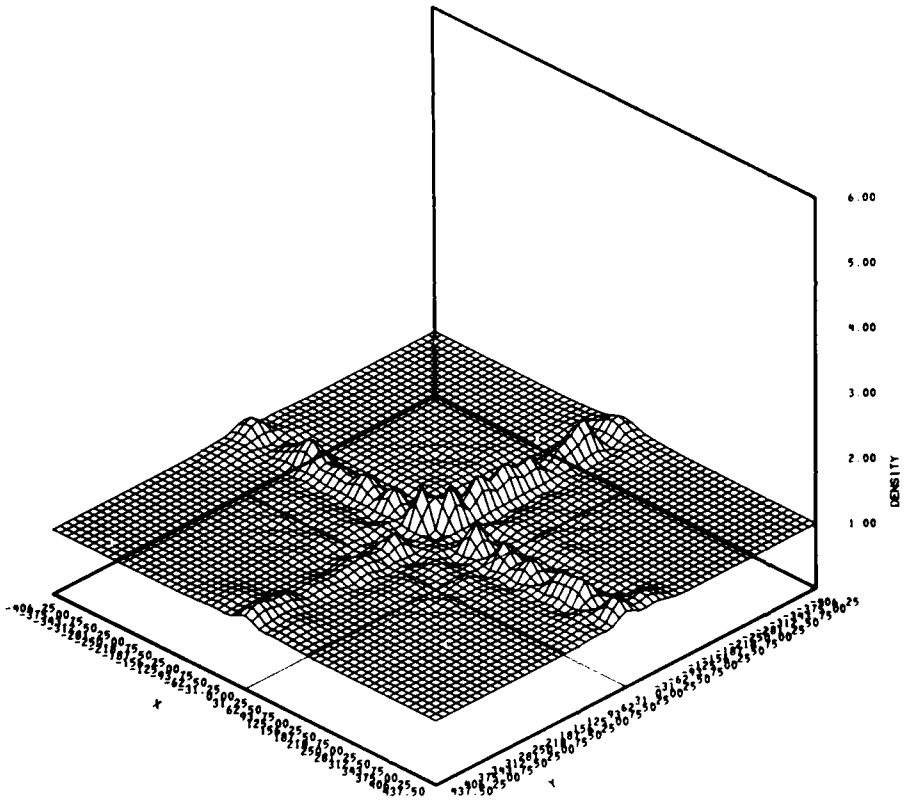

Figure 6K. Case I - plasma density - 6000 seconds.

There appear to be three issues raised by the results of the first case which require further thought. First, if the mixing model were absolutely symmetric, the macroscopic fingers would not have occurred. Thus, future work needs to evaluate the importance of using the more elaborate 13-point model mentioned in an earlier section. On the other hand, no finite difference procedure can be absolutely "smooth" and, perhaps, the results are merely exaggerating a discrepancy in the modelling which needs specific attention. In particular, we identify a second topic as the question of whether the macroscopic motion should be able to "outrun" the mixing regardless of the perturbation produced. Conceptually, it seems that the "mixing front" ought to proceed at about the same pace as a "macroscopic finger front". The two are, in fact, supposed to represent the same physical phenomenon and the specific coupling to the wind is not dependent on scale size to first order.

The third issue raised by the results of the first case is the virtual uniqueness of the initial condition, which produces no gross macroscopic motion. In any real scenario, there would not be complete axisymmetry and the gross motion would undoubtedly wash out perturbations produced by the mixing model. The purpose of case two is to explore this issue in more detail.

In the second case, we start the computation with the same basic wind and cloud, but now the cloud is offset diagonally from the center by 100 units. The initial plasma distribution is seen in Figure 7A. By 600 seconds, a significant macroscopic velocity (caused by the offset) has pushed the cloud into a barium release type configuration, as seen in Figure 7B. The microstructure power distribution at this time, as displayed in Figure 7C, is quite different than the earlier case. As expected, however, its intense region

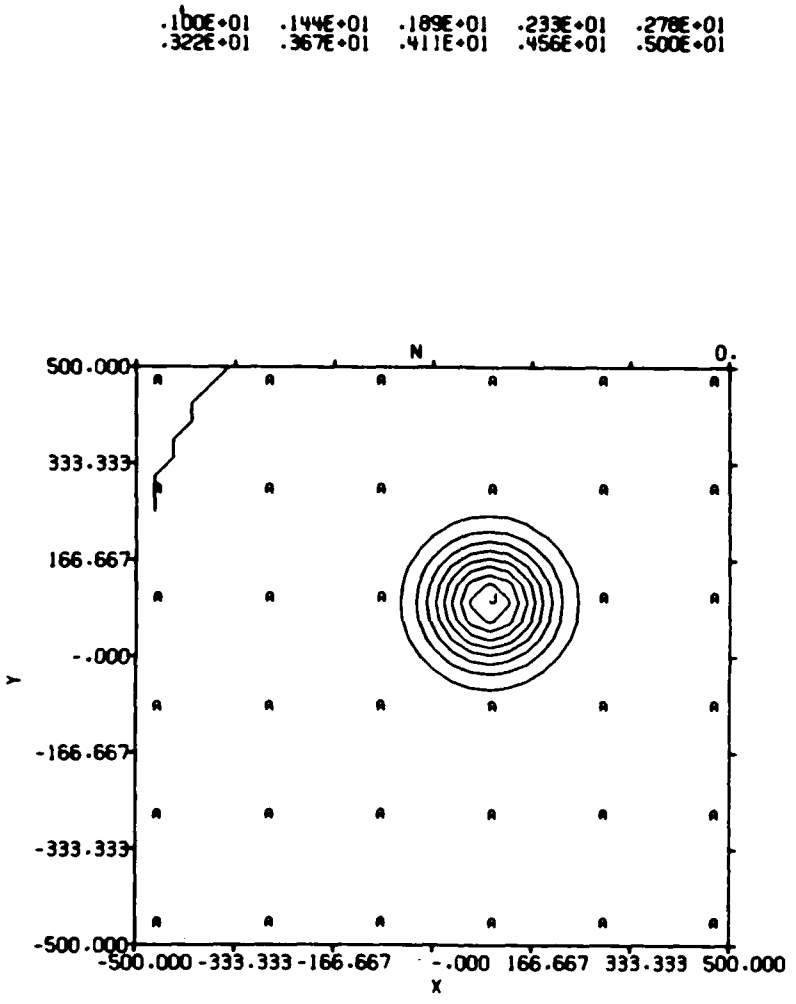

Figure 7A. Case II - plasma density - 0 seconds.

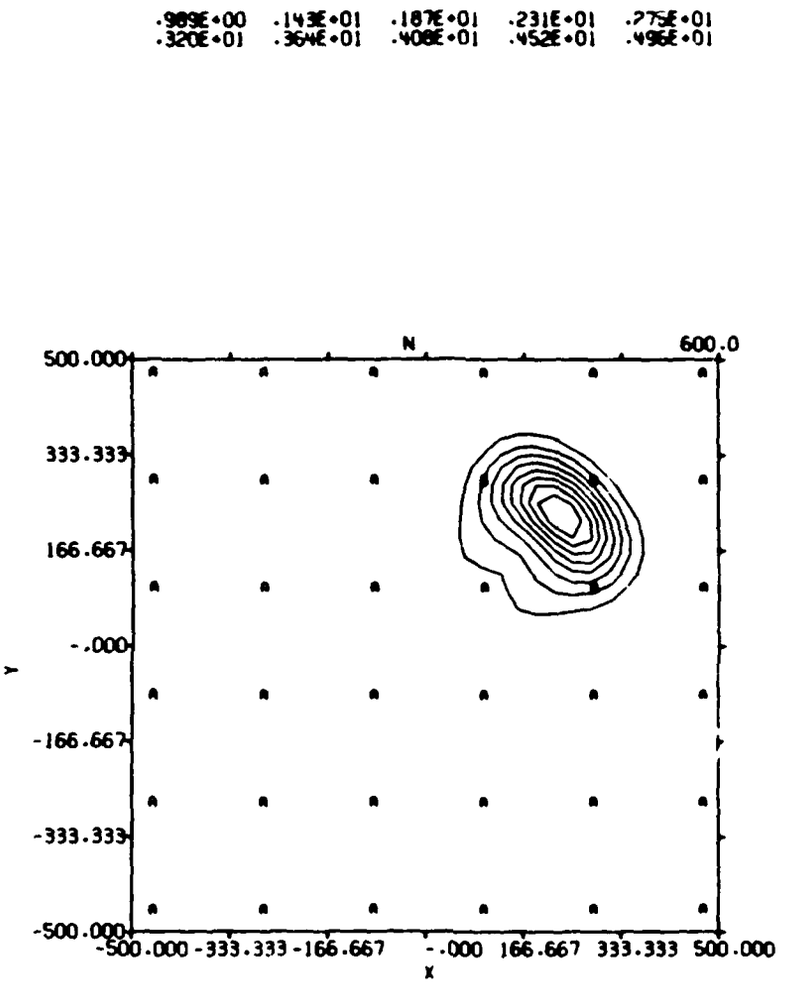

Figure 7B. Case II - plasma density - 600 seconds.

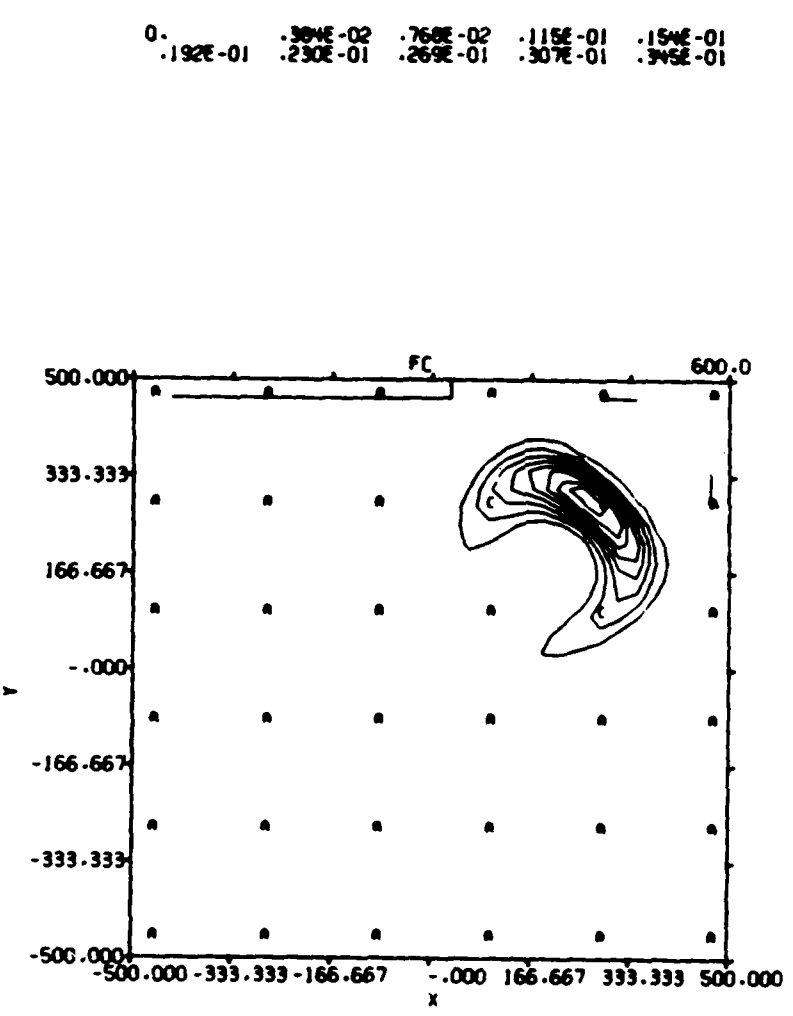

Figure 7C. Case II - microstructure power - 600 seconds. Peak F_C = .0346.

is centered on the edge pointed with the neutral wind. The convection of microstructure, forming tip wakes, is evident in the figure. Figure 7D is the 3-D plasma plot at 100 seconds, whereas Figure 7E is the further evolution at 400 seconds.

At 800 seconds, in Figure 7F, the cloud has reached the boundary and is starting to leave the grid. We should note two things about the figure. First, as expected, there are no "cross-like" perturbations. The macroscopic motion has clearly washed them out. Second, at this last time frame, before the cloud leaves the grid, there is not much evidence of peak density decay. It is not clear that the mixing has played a significant role in the cloud evolution. Whether it should have played a role, at this particular time, is not clear from our experimental knowledge of such clouds. We do wonder, however, as in case one, if the mixing has been "too weak" to keep pace with the macroscopic motion.

Figures 7G, 7H, and 7I display the ultimate macroscopic convection of the case two cloud out of the grid. While interesting in displaying the ability of the numerical techniques to handle the task, they shed little light on the specific influence of striation convection.

In the course of the present work, we have simultaneously begun the research and development on the new microstructure model mentioned in the Appendix. One of the early observations was that, while the simple model generally agreed in qualitative format with the new results, it consistently produces much lower levels of microstructure. Thus, it occurred to us that we ought to try the mixing routine using artificially augmented microstructure rates in the simple model. Using some modifications to the factors β_1 and β_3, we can make the simple microstructure model come closer to the new research

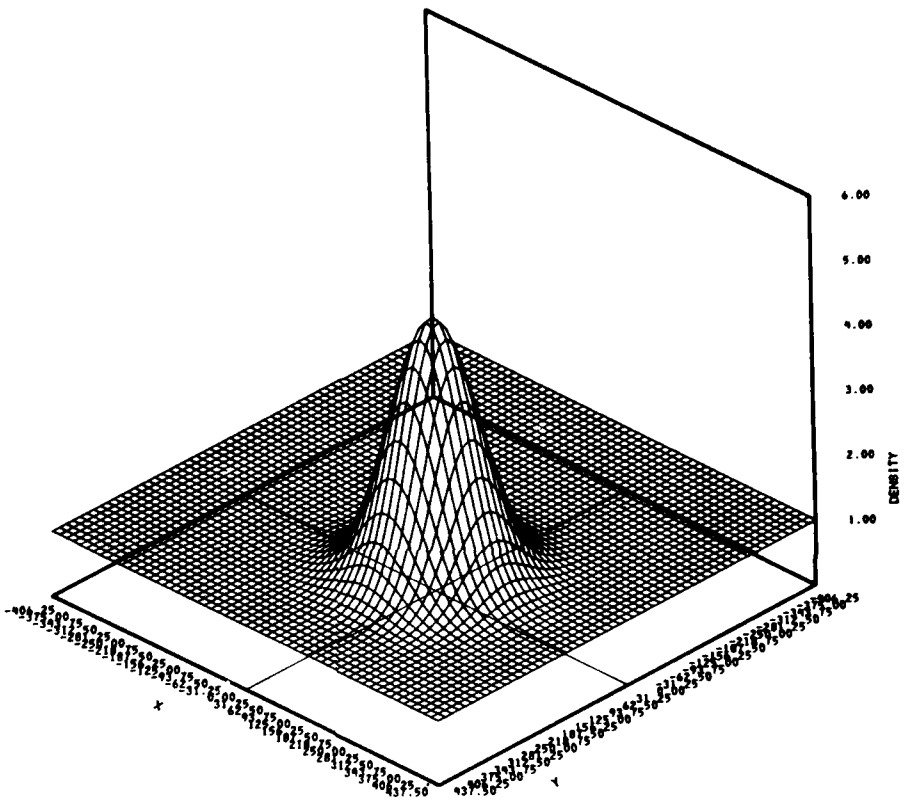

Figure 7D. Case II - plasma density - 100 seconds.

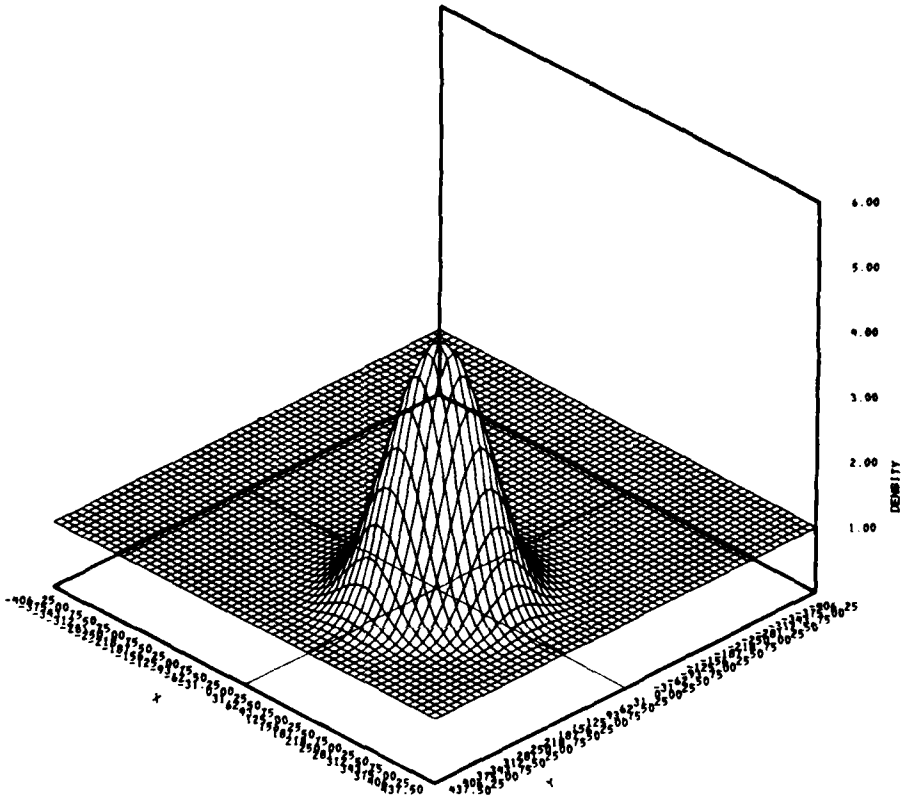

Figure 7E. Case II - plasma density - 400 seconds.

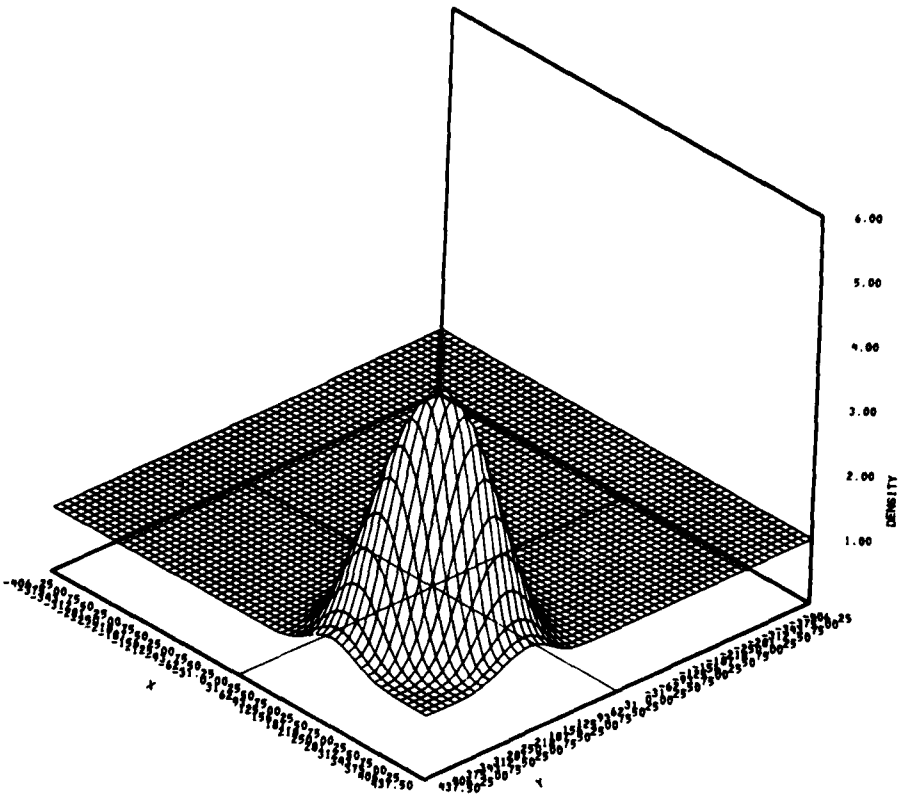

Figure 7F. Case II - plasma density - 800 seconds.

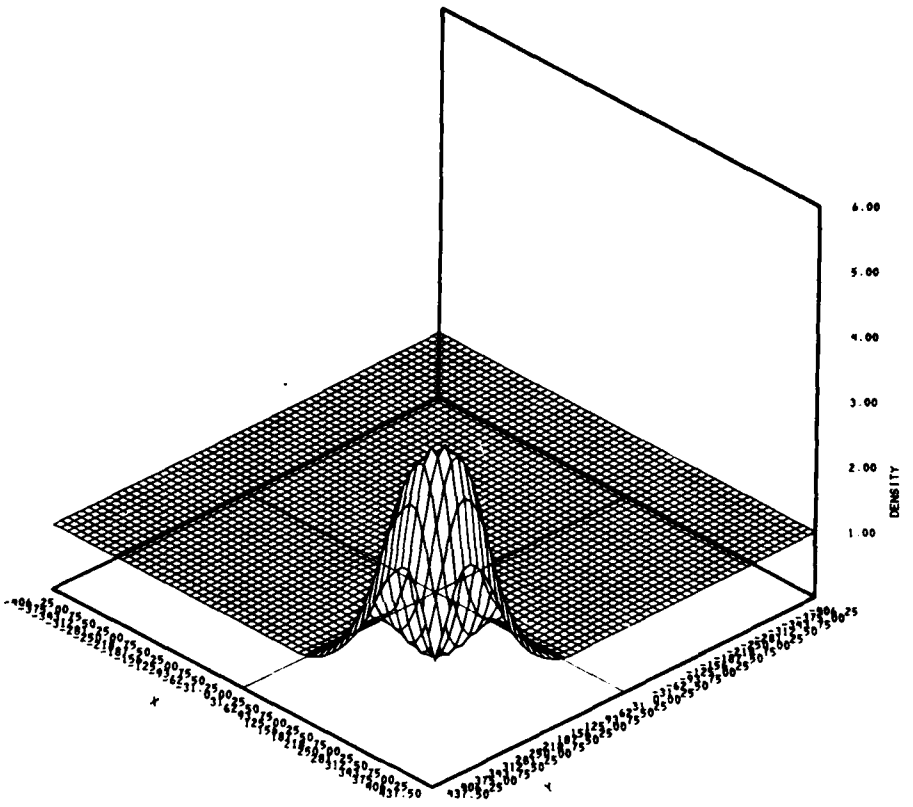

Figure 7G. Case II - plasma density - 1200 seconds.

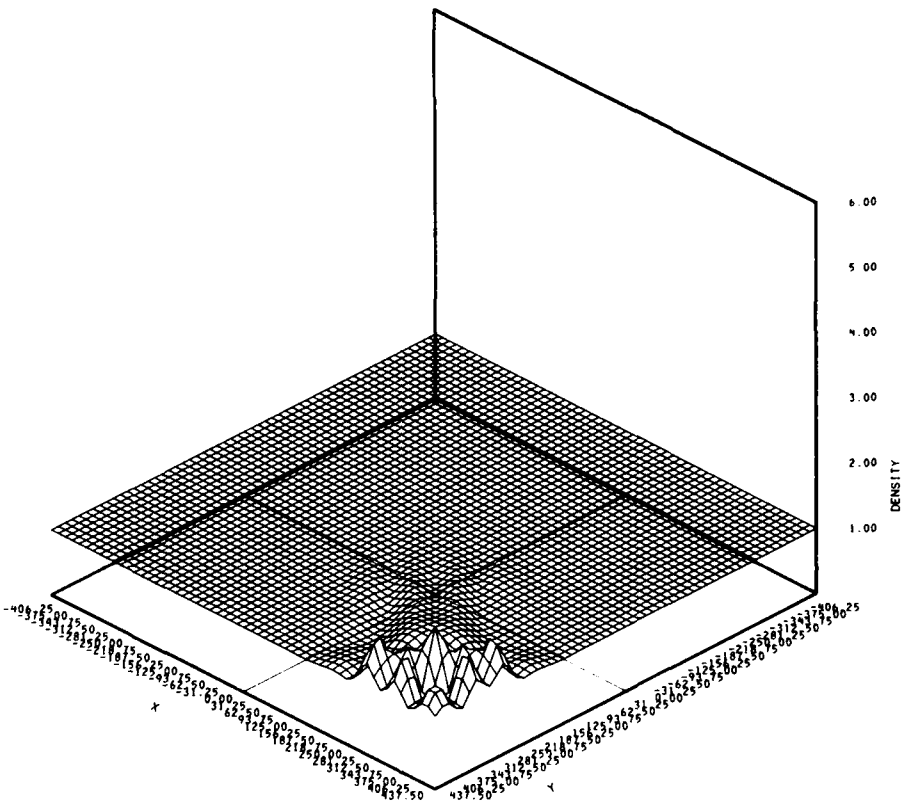

Figure 7H. Case II - plasma density - 1600 seconds.

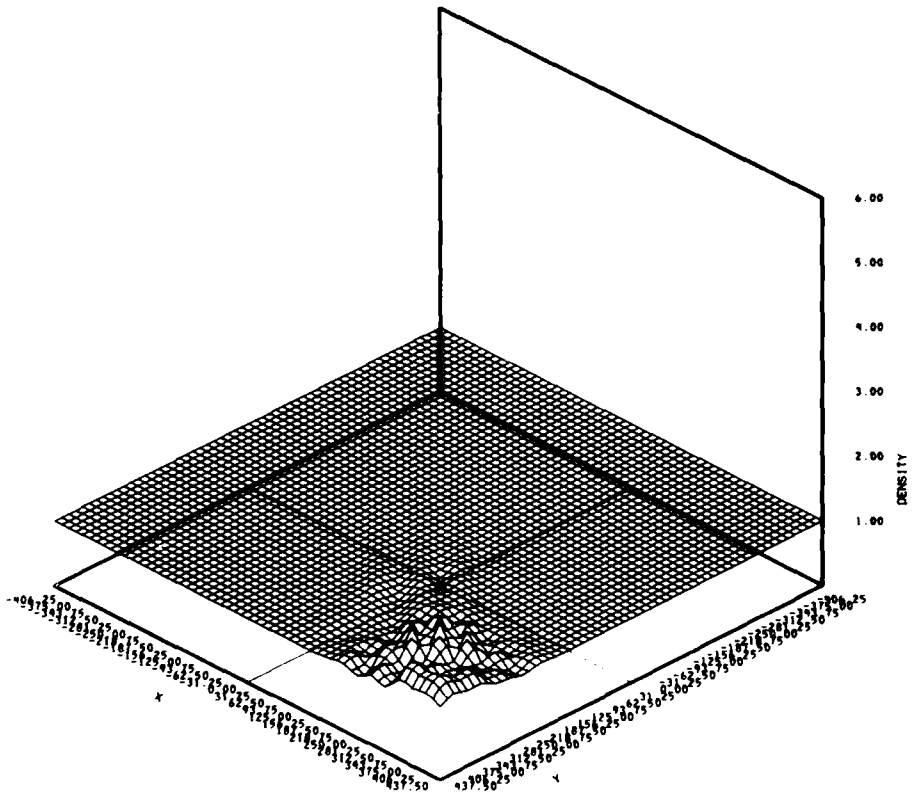

Figure 7I. Case II - plasma density - 3000 seconds.

results. (Cases I and II were run with $\beta_1 = \beta_3 = 1.$) For purposes of the present work, the details are unimportant, but the fact of augmentation in F_C as a qualitative feature is the issue. The third case is a rerun of case one with artificially augmented F_C ($\beta = 10$).

Figure 8A is a 2-D plot of plasma density in Case III at 100 seconds. We may note that the peak central density has already been reduced to 4.97 from 5.00. Of prime interest is Figure 8B, which shows F_C at 100 seconds. Comparison with Figure 6C for Case I at 600 seconds indicates that the peak values for F_C are more than seven times larger, even though the time is six times shorter. The 3-D density plot at 100 seconds is shown in Figure 8C.

The evolution of plasma in Case III is very rapid, as displayed in Figures 8D, 8E, 8F, and 8G at 200, 300, 400, and 500 seconds respectively. The artificially high rate of microstructure growth speeds up the mixing and rapidly dissipates the cloud. Even in the stationary environment, the process is relatively smooth compared to the earlier Case I. Clearly, the mixing has completely overwhelmed the macroscopic motion in this example. While there is some evidence of the cross pattern in Case III, we would conclude that the bulk of the effect in Case I was due to augmentation by the potential solver.

The tuning of future microstructure models to provide consistent motion between the striation convection front and the macroscopic feature front is probably an important consideration.

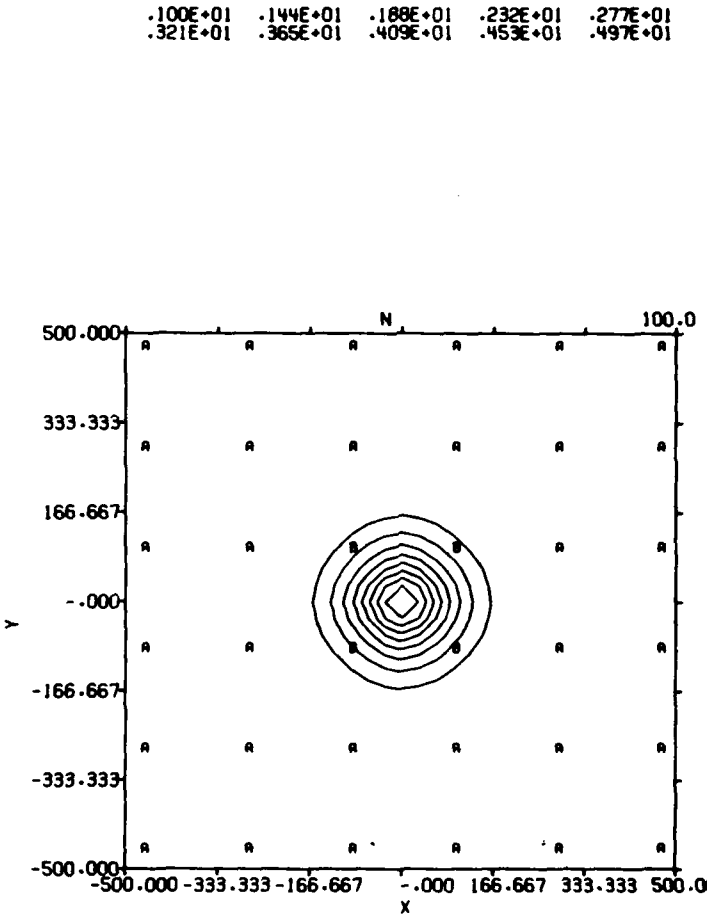

Figure 8A. Case III - plasma density - 100 seconds.

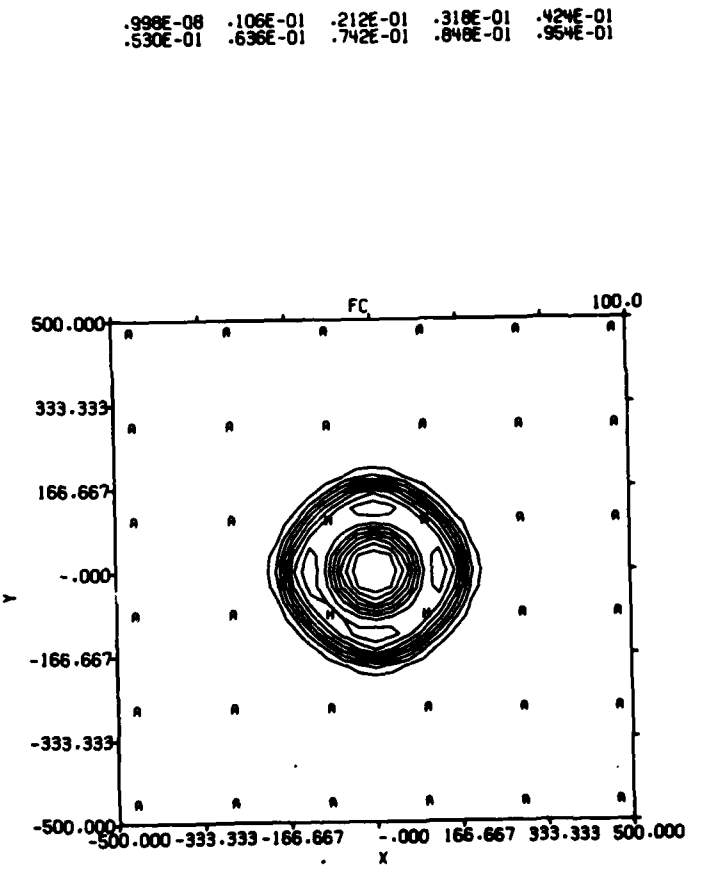

Figure 8B. Case III - microstructure power - 100 seconds. Peak F_C = .0954.

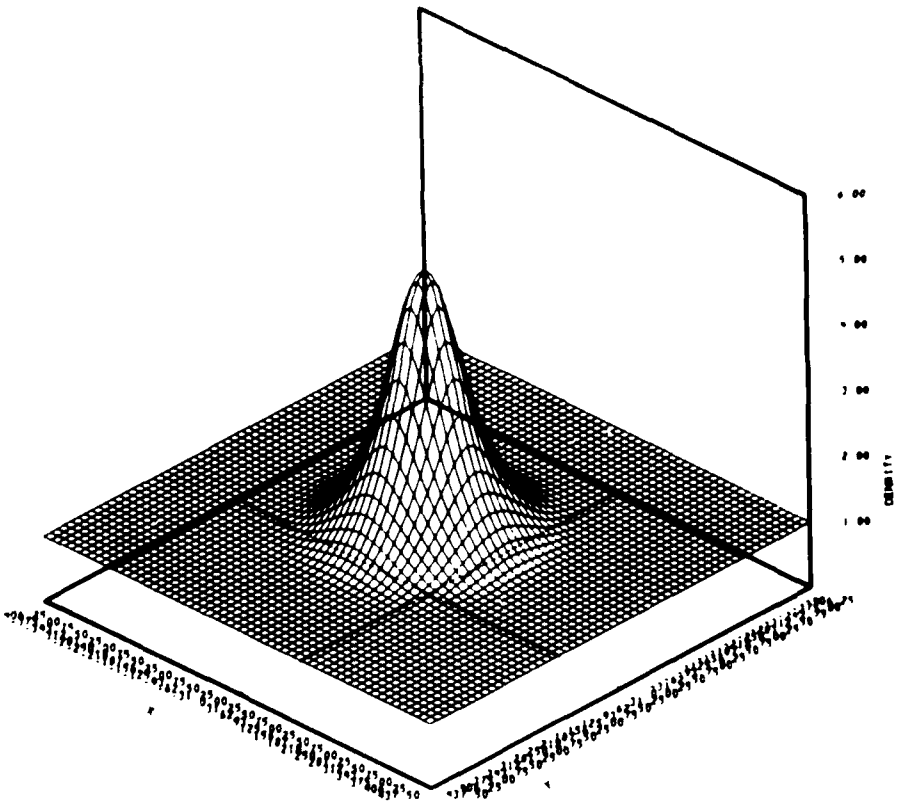

Figure 8C. Case III - plasma density - 100 seconds

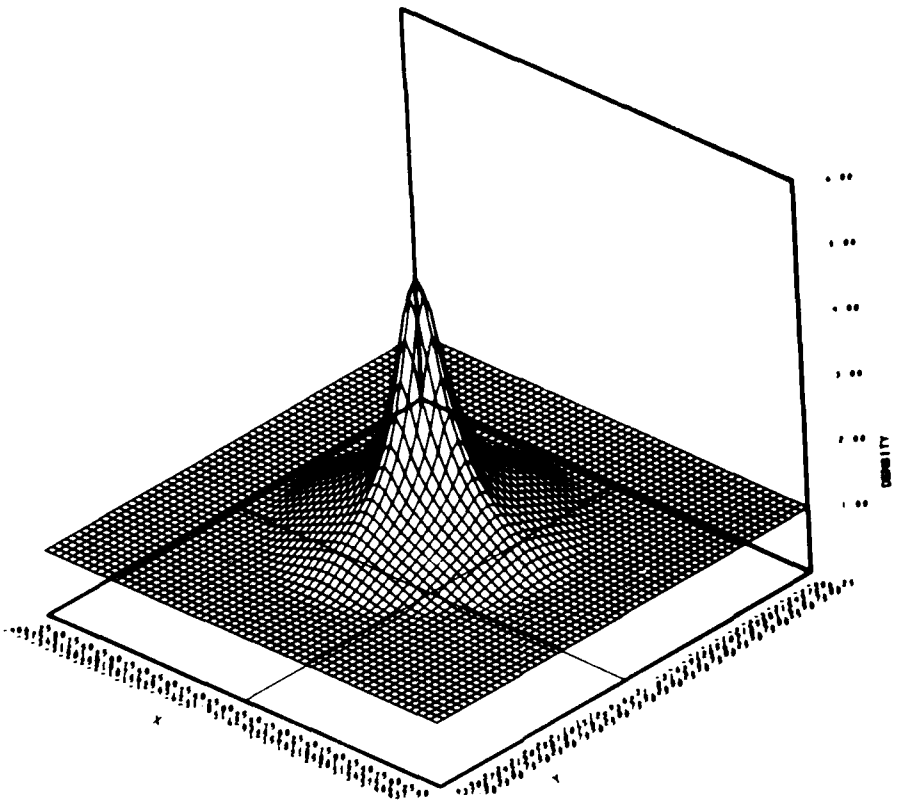

Figure 8D. Case III - plasma density - 200 seconds.

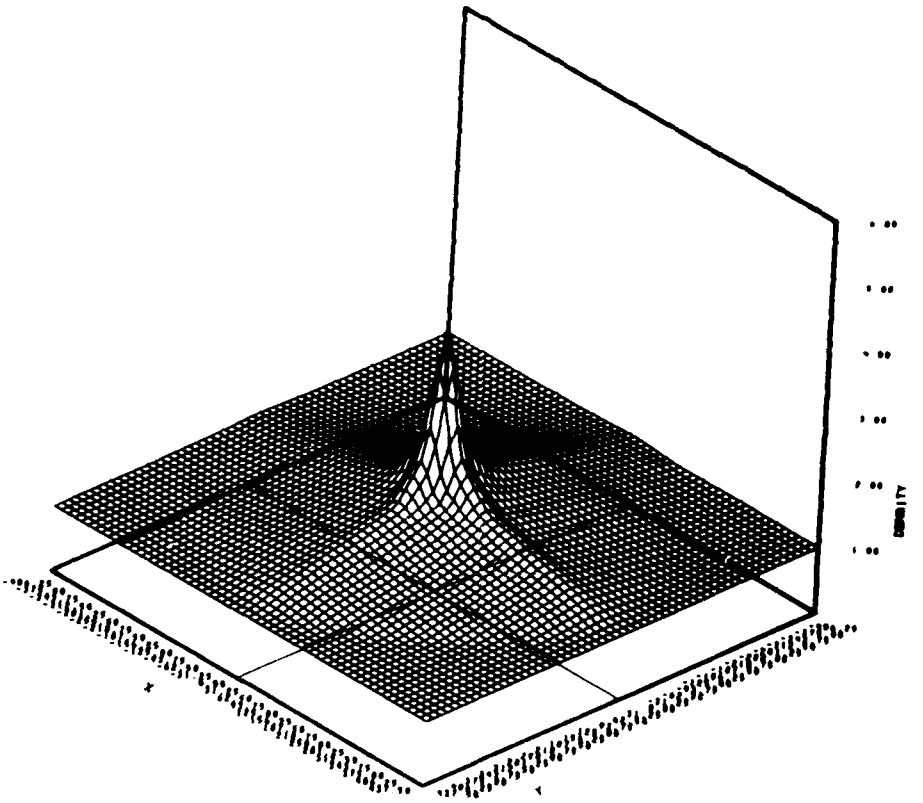

Figure 8E. Case III - plasma density - 300 seconds.

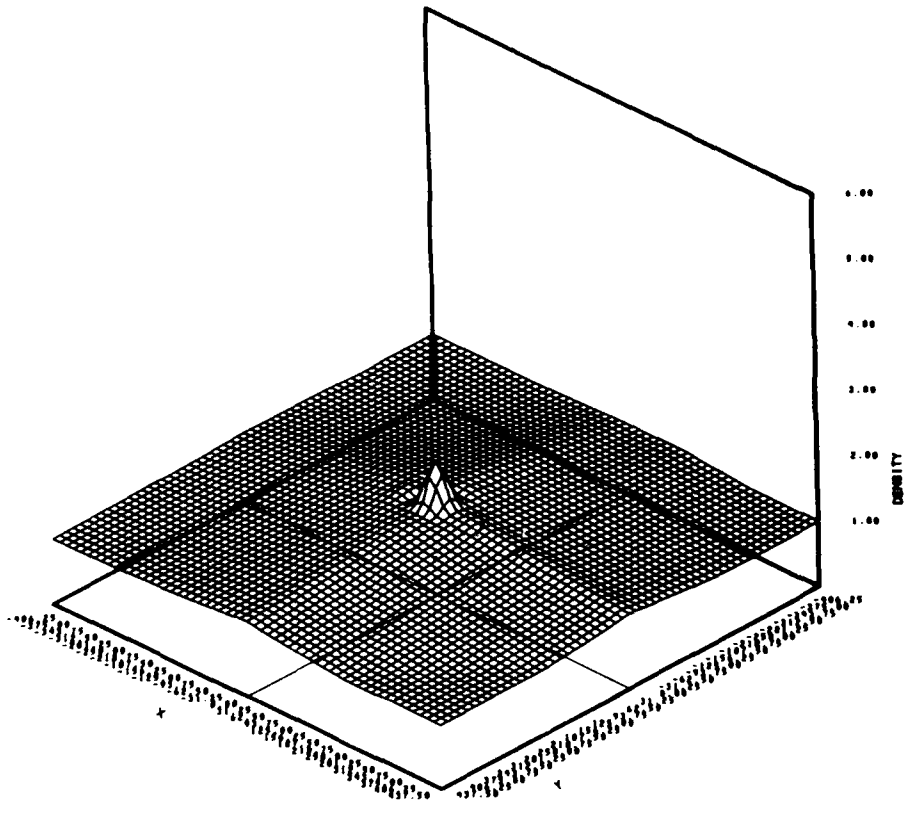

Figure 8F. Case III - plasma density - 400 seconds.

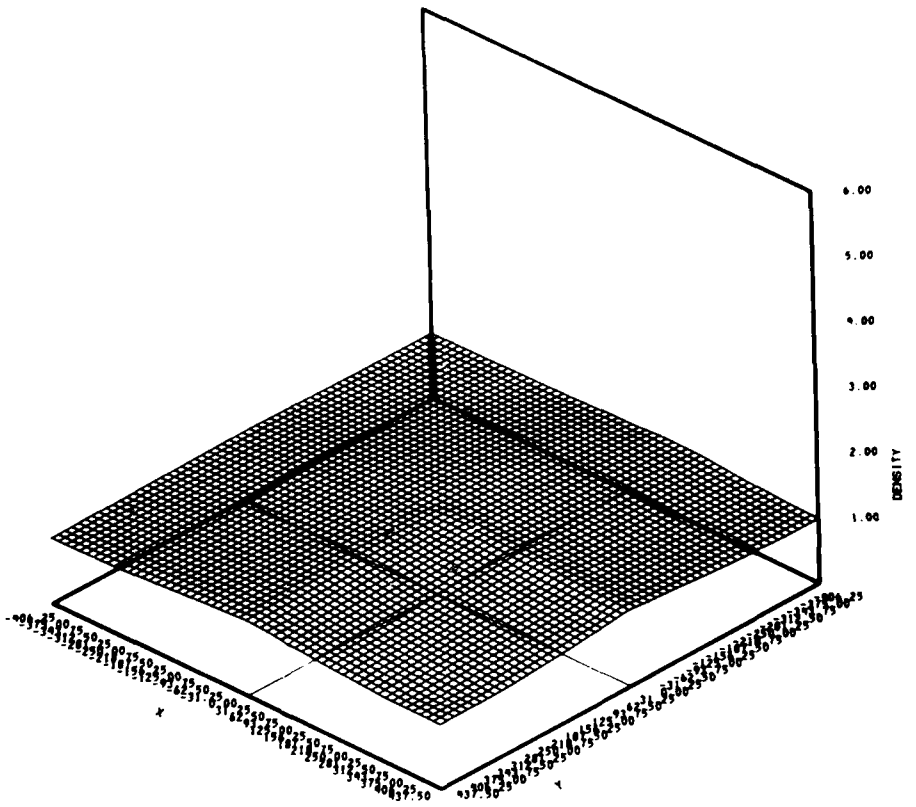

Figure 8G. Case III - plasma desnity - 500 seconds.

SECTION V
CONCLUSIONS

The use of power conservation to construct a mixing model representation of striation convection appears to be quite successful. The qualitative features are in agreement with the expected behavior of such physics. With the future use of an advanced microstructure routine and integration with experimental data, we believe that satisfactory quantitative results are possible. The procedure will shortly be added to the SCENARIO systems analysis code and provide a great increase in ability to run to late times. We would recommend that the model should be added to research codes such as MELT and MAGIC.

As indicated in the commentary of the text, there are a variety of studies and tasks which would enhance the understanding and general credibility of the technique. At least for research purposes, the development and utilization of a more symmetric 13-point model ought to be explored. The chief area of work, however, should focus on the close dependence with microstructure rates and the implications in more general scenarios.

Clearly, the detailed research and development required for deployment in the full three-dimensional environment remains relatively unexplored. Striation convection under the influence of gravity and inertial forces are topics for future work.

SECTION VI

REFERENCES

1. Workman, J.B., and S.Y.F. Chu, A Gradient Drift Microstructure Model, DNA 4539T, February 1978.

2. Workman, J.B., J.A.L. Thomson, and S. Singer, A Plasma Model for the Disturbed Environment, DNA 3613T, December 1974.

3. Wittwer, L.A., private communication.

SECTION VII
APPENDIX - SIMPLE MICROSTRUCTURE MODEL

Initially, when the construction of the mixing model was undertaken, it was assumed that it would be coupled directly to the microstructure model of Reference 1. It appeared reasonable, however, to make available a simple model for both quick running and easily visualized behavior during code construction and refinement. Recently, however, guided by some astute observations on the true physics of outer scale behavior by Wittwer,[3] we have undertaken a significant revision of the initial code. Interestingly enough, the simple model to be described here is phenomenologically closer to the new code than the old. The end result of all of these considerations is that we have chosen to use the simple code in generating the results in the present study instead of the more complex model of Reference 1.

Assuming that the reader is either familiar with the earlier work or can make reference to it,[1] the construction of the simple model is straightforward. Essentially, we assume that both the outer scale and inner scale are fixed. Thence, we consider <u>only</u> the cascade regime of power. That is, all of the microstructure power to be treated in the problem is assumed to be F_C. There is only <u>one</u> rate relation and it refers to this specific regime (Equation 79 of Reference 1).

$$\frac{1}{2}\frac{dF_C}{dt} = (\Delta U)\, k_o \sqrt{F_o}\left[F_C + \beta_1 F_o \left(\frac{k_o}{\bar{k}_C}\right)\right] - \beta_3 (\Delta U)\, \bar{k}_C F_C \sqrt{F_C}\,\frac{\bar{k}_C}{\bar{k}_D} \qquad \text{(A-1)}$$

The constitutive relations then become

$$\bar{k}_C = \sqrt{k_D k_R}$$

$$\bar{k}_D = (5/3)^{\frac{1}{2}} k_D \qquad \text{(A-2)}$$

$$k_D = Q k_R$$

where k_R is now the fixed outer scale wavenumber, k_C, corresponding to the cell grid dimension parameter

$$k_R = 2k_o = \frac{2\sqrt{3}}{L} \qquad \text{(A-3)}$$

The inner scale wavenumber, k_D, is fixed at some multiple Q of k_R. For purposes of the present study, Q is fixed at 1000.

The rate coefficients β_1 and β_3 are initially taken as unity, but then varied as discussed in the results section.

DISTRIBUTION LIST

DEPARTMENT OF DEFENSE

Assistant to the Secretary of Defense
Atomic Energy
ATTN: Executive Assistant

Defense Nuclear Agency
ATTN: STVL
ATTN: DDST
3 cy ATTN: RAAE
4 cy ATTN: TITL

Defense Technical Information Center
12 cy ATTN: DD

Field Command
Defense Nuclear Agency
ATTN: FCPR

Field Command
Defense Nuclear Agency
Livermore Division
ATTN: FCPRL

Undersecretary of Defense for Rsch. & Engrg.
ATTN: Strategic & Space Systems (OS)

DEPARTMENT OF THE ARMY

BMD Advanced Technology Center
Department of the Army
ATTN: ATC-O, W. Davies
ATTN: ATC-T, M. Capps
ATTN: ATC-R, D. Russ

Harry Diamond Laboratories
Department of the Army
ATTN: DELHD-N-P

DEPARTMENT OF THE NAVY

Naval Research Laboratory
ATTN: Code 6700, T. Coffey
ATTN: Code 7500, B. Wald
ATTN: Code 7550, J. Davis
ATTN: Code 6780, S. Ossakow

Naval Surface Weapons Center
ATTN: Code F31

DEPARTMENT OF THE AIR FORCE

Air Force Geophysics Laboratory
ATTN: PHP, J. Aarons

Air Force Weapons Laboratory
Air Force Systems Command
ATTN: SUL
ATTN: DYC

DEPARTMENT OF ENERGY CONTRACTORS

Los Alamos Scientific Laboratory
ATTN: Document Control for D. Simons

DEPARTMENT OF DEFENSE CONTRACTORS

Berkeley Research Associates, Inc.
ATTN: J. Workman
ATTN: S. Chu
ATTN: J. Ferrante

ESL, Inc.
ATTN: J. Marshall

General Electric Company—TEMPO
ATTN: W. Knapp
ATTN: T. Stevens
ATTN: DASIAC

General Research Corp.
ATTN: J. Garbarino
ATTN: J. Ise, Jr.

University of Illinois
ATTN: Security Supervisor for K. Yeh

JAYCOR
ATTN: S. Goldman

Mission Research Corp.
ATTN: R. Kilb

R & D Associates
ATTN: C. MacDonald

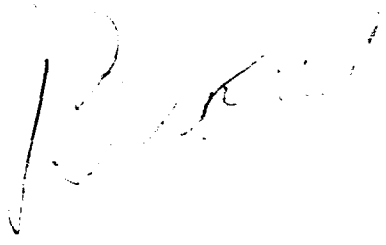

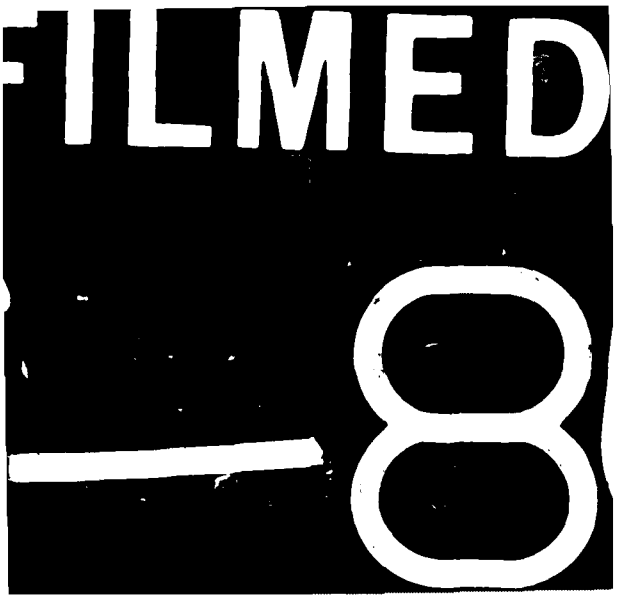
FILMED
8